Chapter 2 Part A

Hydrogen Bond Synthon Competition in the Stabilization of Theophylline Cocrystals

2.A.1 Abstract

Seven new cocrystals/salt of bronchodilator drug theophylline are synthesized by considering phenols and isomeric hydroxybenzoic acids as coformers. Solvent-assisted mechanochemical grinding has been used to synthesize these cocrystals. Materials are characterized by using thermal, spectroscopy, powder X-ray diffraction techniques. Single crystal structures are obtained for all the cocrystals. The stability of these cocrystals at various relative humidity is determined. Aqueous solubility is evaluated for each cocrystal and compared with the parent drug. The present study shows the cocrystals with phenolic coformers are less stable towards high humid condition and exhibit better aqueous solubility compared to the cocrystal with hydroxybenzoic acids. The stability and solubility behaviour of the cocrystals are accounted with the hydrogen bonding synthon present and crystal packing features. The existence of weaker O−H···N$_{imidazole}$ hydrogen bond synthon in the cocrystals with phenolic coformers facilitates for higher solubility and lesser stability. However, the presence of –COOH group prevents water incorporation as it involves in the formation of stronger COOH···N$_{imidazole}$ synthon and thereby provides additional physical stability to the cocrystal. Results show the feasibility of cocrystal design of a drug to tune physiochemical properties based on hydrogen bond synthon formation.

2.A.2 Introduction

Cocrystallizing an API with a pharmaceutically acceptable molecule has boosted the attractive route for developing pharmaceutical products. Synthesis of cocrystals is important because it can modulate physiochemical properties of the parent drug, particularly the solubility, dissolution profile, stability and therefore became the routine practice among pharmaceutical researchers [1–9]. Since last two decades, several researchers have been actively involved in investigating the property modulation of a drug by employing cocrystallization technique. But the property prediction of the drug-cocrystal based on hydrogen bond and coformers is still a debate. Coformer selection

plays a vital role in determining the cocrystals properties. The presence of different functional groups in coformer produce different hydrogen bond synthon in cocrystals and consequently differ in their properties [10–19]. Hence, it is important to select appropriate coformer to design and synthesis of cocrystal which further helps in solving the drug physiochemical issues. Several research groups have studied the hydration stability of theophylline and caffeine cocrystals considering dicarboxylic acids as coformers [20–25] The reported theophylline and caffeine cocrystals with oxalic acid are the most stable among the studied cocrystals in different relative humidity conditions. Rodríguez research group have extensively studied moisture uptake and deliquescence property by highly water-soluble coformers for a series of API cocrystals at different relative humidity conditions [20,24]. The coformer like oxalic acid with high aqueous solubility exhibited the best cocrystal stability at high relative humidity. In contrast, the most soluble and hygroscopic coformers like D-malic acid is found unstable even at 75% RH leading to the hydrated drug. Infantes et al. have examined the factors that determine hydrate formation in organic crystals by exploring the CSD database of reported cocrystals [25]. From this study, they suggested that the donor/acceptor ratio or the molecular weight was not significantly affecting the hydrate formation. However, increasing the polar surface of the molecules might be responsible for a better propensity towards hydrate formation.

This Chapter 2 part A, we explored the cocrystallization strategy to stabilize the drug theophylline based on a coformer selection approach [26]. Understanding the role of coformers and different hydrogen bond synthons in determining the final cocrystal stability, hydration propensity and modulating solubility profile is the prime intention. Theophylline is an active pharmaceutical ingredient (API) analogous to caffeine and theobromine which belongs to the xanthine family and considered as a model drug for the present study [27]. It is used for the treatment of respiratory disease such as chronic obstructive pulmonary disease (COPD) and asthma under the brand name of Choledyl, Elixophyllin, Neulin, Theofyllin, Theochron SR etc. Theophylline is unstable at high humid conditions and behaves in a similar way to caffeine and theobromine towards atmospheric humidity [28]. The instability and interconversion of monohydrate and anhydrous theophylline are reported. The imidazole *N* present in theophylline acts as hydrogen bond acceptor which interacts with atmospheric moisture and thus facilitates

the hydrate formation [24,28]. Therefore, by preventing the formation of weak hydrogen bond synthon i.e. O−H···N$_{imidazole}$ through replacing it via the formation of stronger COOH···N$_{imidazole}$ synthon, the instability of this molecule can be overcome.

2.A.3   Results and Discussion

2.A.3.1 Synthesis of Cocrystals

Several phenols such as resorcinol (Res), orcinol (Orc), phloroglucinol (Phu), and isomeric dihydroxybenzoic acids such as 2,6-dihydroxybenzoic acid (2,6-DHBA), 3,4-dihydroxybenzoic acid (3,4-DHBA) and 3,5-dihydroxybenzoic acid (3,5-DHBA) are considered as coformers to synthesize cocrystals with theophylline (Scheme 2.A.1). Cinnamic acid (CA) is also considered under the category of the aromatic carboxylic acid with no –OH group.
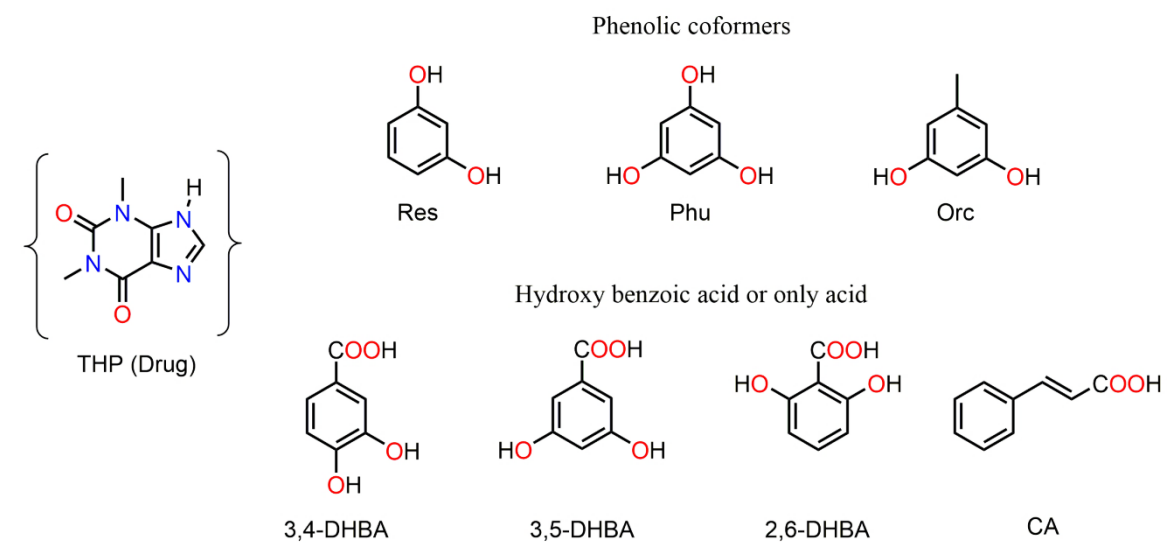
Scheme 2.A.1 Chemical structures of API theophylline and the coformers.

Coformers with carboxylic acid functionality are suitable for cocrystal formation as –COOH can act either as a hydrogen bond acceptor (C=O, the carbonyl) or as a hydrogen bond donor (−OH, the hydroxyl). The API theophylline behaves in an identical manner. The imidazole −NH and the =CH group of THP can act as hydrogen-bond donors. The imidazole N. and two carbonyl oxygen atoms act as hydrogen-bond acceptors. Theophylline and its analogous caffeine and theobromine involve in cocrystallization by the formation of strong hydrogen bonds O−H···O, N−H···O, O−H···N with dicarboxylic

acids such as oxalic acid, maleic acid, glutaric acid, dipicolinic acid, pyrazole dicarboxylic acid, trimellitic acid and reported elsewhere [28,29]. Alike to compounds containing –COOH functional group, compounds comprising phenolic −OH group are also competent coformers for cocrystal design. However, phenols demand compensation of hydrogen bond formation with theophylline which may be feasible by the inclusion of water or solvent molecules into the crystalline lattice. Being deficient in hydrogen bond acceptor phenols could result in inefficient intermolecular interactions between molecules. Therefore hydrogen bond donor-acceptor ratio is adjusted for these cocrystals by the inclusion of water molecules into the crystalline lattice.

Table 2.A.1 Synthesis of seven new cocrystals of drug theophylline with phenols and isomeric dihydroxybenzoic acids with 1:1 ratio. Cocrystals **1**, **2**, **3**, **4** are hydrates.

Cocrystal	Components	Stoichiometry	Abbreviation
1	THP + Resorcinol+H_2O	1:1:1	THP·Res·H_2O
2	Theophylline + Phlouroglucinol+H_2O	1:1:1	THP·Phu·H_2O
3	Theophylline +Orcinol+H_2O	1:1:2	THP·Orc·$2H_2O$
4	Theophylline + 2,6-Dihydroxybenzoic acid +H_2O	1:1:1	THP·2,6-DHBA·H_2O
5	Theophylline + 3,5-Dihydroxybenzoic acid	1:1	THP·3,5-DHBA
6	Theophylline + 3,4-Dihydroxybenzoic acid	1:1	THP·3,4-DHBA
7	Theophylline +Cinnamic acid	1:1	THP·CA

Present investigation emphasizes the importance of understanding the factors that contribute to the tailoring physical stability of theophylline cocrystals with different isomeric dihydroxybenzoic acids compared to phenolic coformers. This study of strategic coformer selection for cocrystal synthesis to modulate physical properties of theophylline drug aims at the following objectives, (i) liquid assisted mechanochemical grinding to formulate new cocrystals [30,31] (ii) to achieve physical stability of cocrystals of theophylline even at high humid conditions that may improve efficacy and storage performance of a drug, (iii) to determine aqueous solubility profile of the cocrystals and correlate it to hydrogen bond synthon energies, and (iv) to predict the formation of salt vs. neutral cocrystal materials based on $\Delta p\mathrm{K_a}$ rules [31–33].

An ionic molecular adduct is produced on cocrystallization of theophylline with 2,6-dihydroxybenzoic acid. However, other coformers furnished neutral cocrystals. Several research groups have thoroughly investigated the reason for the occurrence of neutral or ionic hydrogen bond in acid-base complexes [14,33–35]. The proton transfer behaviour in carboxylic acids and pyridine molecular complexes was emphasized on the difference in pK_a between the base and acid. The $\Delta pK_a < 0$ and >4 for acids and bases resulted in neutral hydrogen bond and proton transfer situations respectively. When ΔpK_a lies between 0-4, the predictions about ionic and neutral states of the resulting mixture is not assured. Salt formation is predictable for the complex of theophylline ($pK_a = 8.6$) with 2,6-DHBA ($pK_a = 1.26$) due to the larger ΔpK_a value. A comparison of ΔpK_a between theophylline and the isomeric hydroxybenzoic acid those used in this study is depicted in Table 2.A.2. Four complexes (**1**, **2**, **3**, **and 4)** are found to form hydrates. Molecular packing and hydrogen bond synthon behaviour of these cocrystal materials in terms of donor-acceptor ratios are examined. All cocrystal materials comprise only 1:1 ratio of theophylline and respective coformer. Despite taking different starting materials ratios such as 1:1.25; 1:1.5; 1:2; 2:1 of theophylline: coformers, it generates only 1:1 stoichiometry and hydrates for **1-4** (details are in experimental section 2.A.5.2).

Table 2.A.2 pK_a of drug theophylline and the dihydroxybenzoic acid coformers used in this study.

Drug	Coformer	pK_a	$\Delta\,pK_a$	Results
Theophylline ($pK_a = 8.6$)	2,6-Dihydroxybenzoic acid	1.26	7.34	Ionic Complex
	3,5-Dihydroxybenzoic acid	3.61	4.99	Neutral Complex
	3,4-Dihydroxybenzoic acid	4.26	4.34	Neutral Complex
	Cinnamic acid	4.46.	4.14	Neutral Complex

2.A.3.2 Characterization

Seven new cocrystals/salts were synthesized and are characterized by using spectroscopy, X-ray diffraction, and thermal analysis techniques. Preliminary characterization of all these cocrystals is performed by using FT-IR spectroscopy, which is one of the popular analytical techniques and extensively used to study hydrogen bond formation in the cocrystal materials (details are in experimental section 2.A.5.3). Analysing the spectra, asymmetric and symmetric N−H stretching vibrations of cocrystals are observed in the range 3390−3323 cm^{-1} and 3279−3229 cm^{-1} respectively,

due to intermolecular hydrogen bonding. The O−H vibrations appear between 3600−3300 cm^{-1}. The C−N stretching vibrations of imidazole ring are observed within the range of 1350−1220 cm^{-1}, however, C−N for pyrimidine ring appears at 1198, 1166, 1147, 1066 cm^{-1} etc. The N−H stretching vibrations are appeared at lower region due to extended hydrogen bonding in the cocrystal. The C=O stretching are expected for THP at 1715 cm^{-1} and for the carboxylic acid group, it is expected to appear at around 1730−1700 cm^{-1}. However, the C=O appears at lower frequency region as it participates in hydrogen bonding to form the cocrystals. In the cocrystal **4,** interestingly the C=O absorption appeared at much lower region (1560 and 1404 cm^{-1}) which can be assigned as the absorption attributed to the formation of carboxylate ion, COO$^-$ (Figure 2.A.1b).
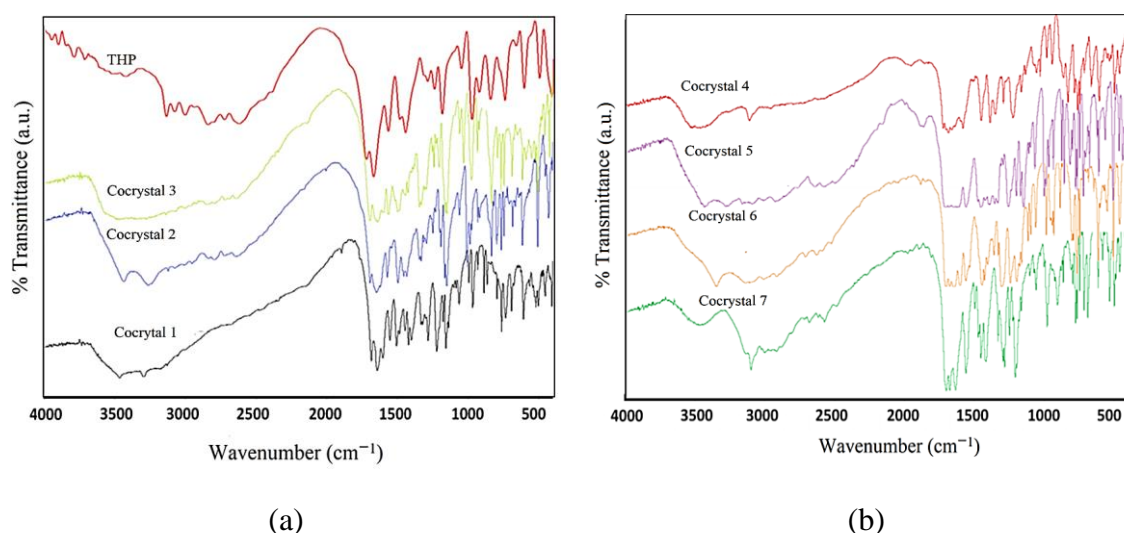

(a) (b)

Figure 2.A.1 FT-IR spectra comparison of theophylline and cocrystals 1-3 (a) and 4-7 (b)

Different thermal analytical techniques such as TGA and DSC are employed to characterize these cocrystals. The endotherm corresponding to water loss was observed by DSC for all the hydrate structures (Figure 2.A.2). The onset of melting and peak observed by DSC for cocrystal materials is presented in Table 2.A.3. All the cocrystal materials exhibit different melting behaviour compared to the parent API and coformers. This indicates the formation of pure phases of cocrystals. For cocrystal 1 and 3 water loss and melting endotherms are observed relatively at a lower temperature, i.e. ~80 °C & ~50 °C and 101 °C & 109 °C respectively. An endotherm at 112 °C for cocrystal 2 indicates water loss, however, the cocrystal material melts at 153 °C. Recrystallization of

this material followed by recording DSC reveals a second endotherm for cocrystal 2 at 169 °C may be due to phase transformation into anhydrous or an unknown form. Broad endotherm for cocrystal **3** corresponds for two water molecules lost at relatively low temperature.
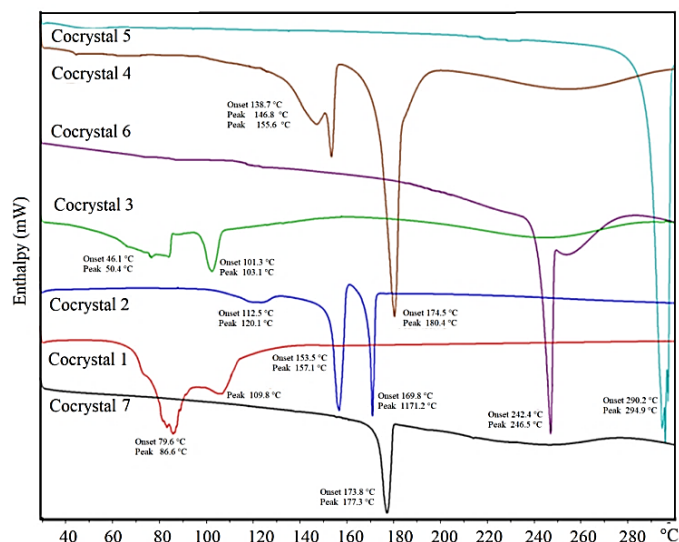

Figure 2.A.2 Differential Scanning Calorimetry (DSC) of cocrystals **1**, **2, 3** and **4** show corresponding endotherm for water loss. Melting temperature for all cocrystal materials were found different from the starting materials.

Table 2.A.3 Comparison of the melting points of the cocrystals (**1**-**7**) with their starting materials.

Drug	Coformer	Coformer MP (°C)	Cocrystals	Water loss Temp.(°C)		Cocrystal MP (°C)	
				Onset	**Peak**	**Onset**	**Peak**
	Res	110-113	**1**	79.6	86.6	101.2	109.8
THP	Phu	218-221	**2**	112.5	120.1	153.1	157.1
[MP~272	Orc	106-112	**3**	46.1	50.4	101.1	103.1
°C)]	2,6-DHBA	165-166	**4**	138.7	146.8	174.5	180.4
	3,5-DHBA	235-238	**5**	–	–	290.2	294.9
	3,4-DHBA	197-200	**6**	–	–	242.4	246.5
	CA	132-135	**7**	–	–	173.8	177.3

Weight loss for water molecules in the hydrate structures were calculated by TGA (Figure 2.A.3). The total weight loss between 50–120 °C is consistent with monohydrate for cocrystals **1** (obs. 5.71%, calc. 5.83%), **2** (obs. 5.34%, calc. 5.53%), **4** (obs. 5.86%, calc. 5.11%) and dihydrate for cocrystal **3** (obs. 11.7%, calc. 10.5%) and confirmed by guest stoichiometry from the X-ray crystal structures that are discussed in later section.
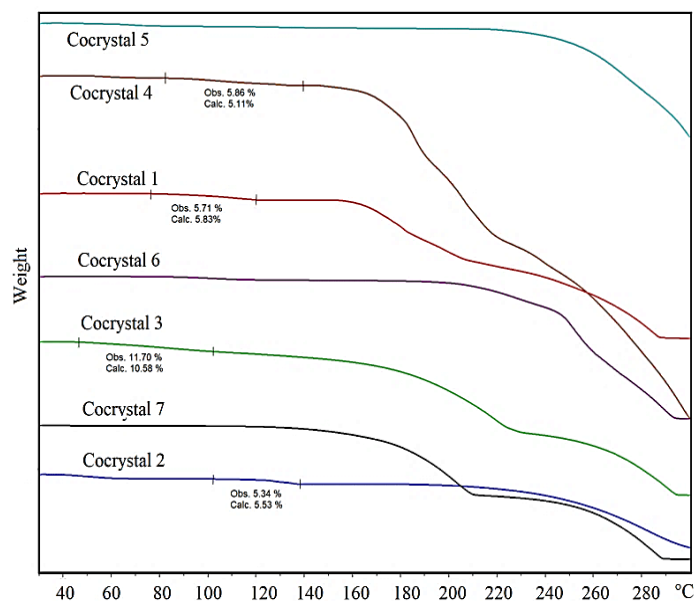
Figure 2.A.3 Quantitative analysis of stoichiometric water in four hydrate structures (**1**, **2**, **3**, **4**) by Thermo Gravimetric (TG) measurement is in accordance with 1:1 ratio determined by single crystal X-ray diffraction.

Cocrystal materials are further analysed by powder X-ray diffraction (details are in experimental section 2.A.5.4). The phase purity of the cocrystals is confirmed by comparing the experimental PXRD patterns of cocrystal **1** to cocrystal **7** with those simulated from the single-crystal structures which are discussed in the subsequent section (Figure 2.A.4).
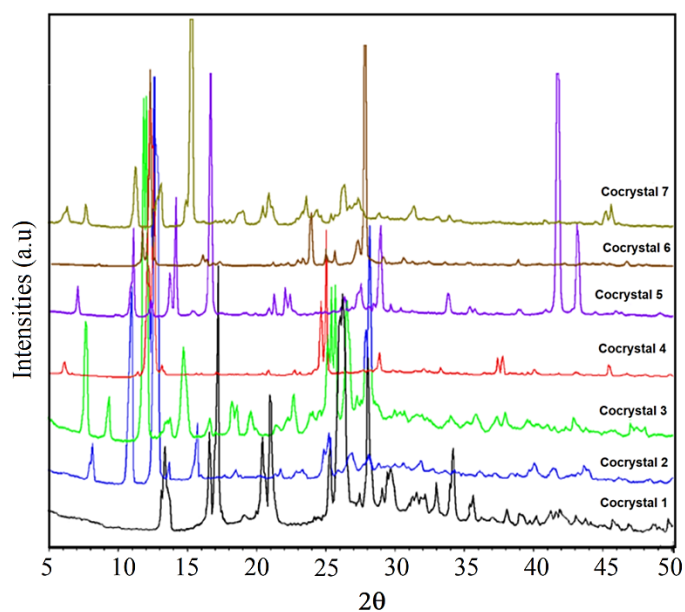

Figure 2.A.4 Powder X-ray diffraction patterns of cocrystals **1**-**7**

A good agreement with the simulated pattern indicated the purity of the phase. The experimental PXRD patterns are overlaid with simulated from crystal structure individually and found in good agreement after Reitvelt refinement [36]. The overlaid patterns are presented in the Appendix Figure A.1.

Single crystal structures for all the cocrystals are evaluated. The crystal data parameters are tabulated in Appendix (Table A.1) and hydrogen bond matrices are listed in Table 2.A.4 along with corresponding symmetry operations.

THP•Res•H₂O [**1**]*: Crystal structure shows that one O−H group of resorcinol interacts with the *exo*-carbonyl of theophylline and imidazole N−H to the O of same OH group. The water molecule is incorporated to adjust H-bond donor-acceptor ratio and acts as a bridge which connects three theophylline molecules and one resorcinol molecule through O−H⋯O, O−H⋯N and N−H⋯O hydrogen bonds nearly in a tetrahedral arrangement (Figure 2.A.5a). The interaction between the resorcinol and theophylline resulted in 3D packing of extended hydrogen bonding where the two components stacked with each other in an alternate fashion (Figure 2.A.5b).

THP•Phu•H₂O [**2**]: Theophylline-phloroglucinol monohydrate single crystals are grown from EtOAc and EtOH solvents. Single crystal data were collected, solved and refined in *P*2₁/*c* monoclinic space group. In absence of strong hydrogen bonding COOH group, the OH groups take part in hydrogen bonding with the *endo*-carbonyl group of theophylline molecule through O−H⋯O hydrogen bond. The other two O−H groups are connected through O−H⋯O hydrogen bond with a water molecule and the adjacent phloroglucinol (Figure 2.A.6a). The imidazole N−H groups form infinite tape through N−H⋯N hydrogen bond with the N1 atom of the adjacent theophylline molecule similar to the anhydrous forms (Figure 2.A.6b).
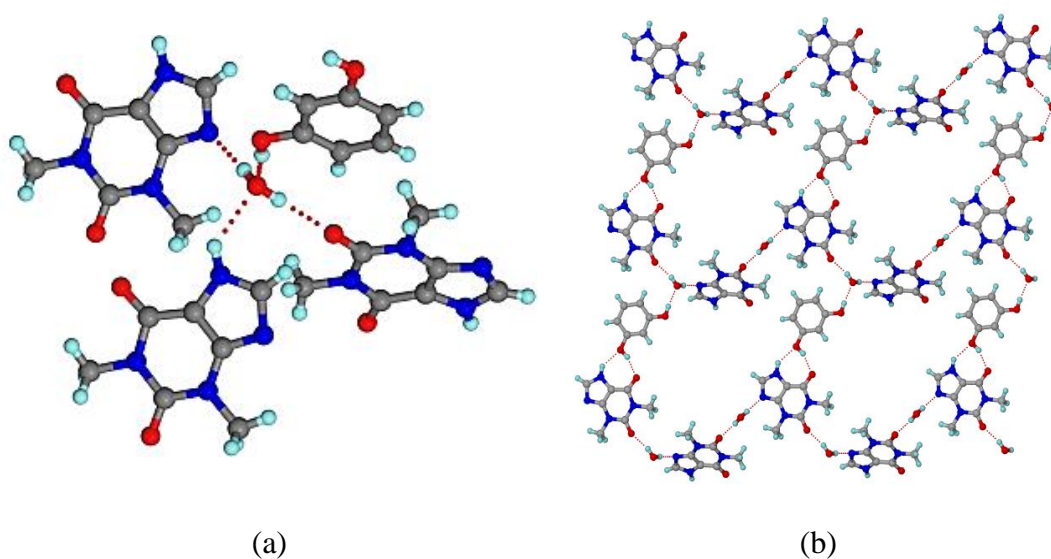
(a)   (b)

Figure 2.A.5 (a) Water acts as connector via O−H···O, O−H···N and N−H···O hydrogen bonds in cocrystal **1**. (b) One of the –OH groups of resorcinol is hydrogen bonded to theophylline through O−H···O and N−H···O from imidazole NH which then extended through water linkage forming a 1D tape. The 1D tapes are connected by theophylline molecule through water linker form 2D net.
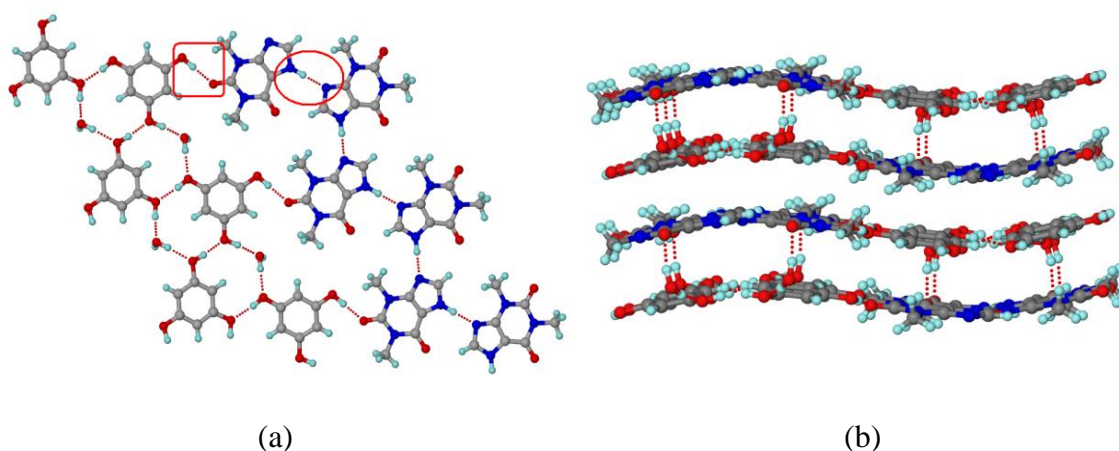

(a)   (b)

Figure 2.A.6 (a) In cocrystal **2**, theophylline forms a catemeric N−H···N hydrogen bonds (synthon E listed in Scheme 2.A.2) found uncommon in theophylline cocrystals. The catemeric N−H···N hydrogen bonds are assisted by weak C−H···O from imidazole =CH. (b) Water molecules connect the wavy 2D molecular sheets to complete 3D packing.

THP•Orc•2H$_2$O [**3**]: Crystal data of **3** were solved and refined in orthorhombic *Pbca* space group. There is no direct interaction between the theophylline and orcinol molecules in the crystal structure; rather they are connected via water molecules via a bifurcation of O−H···O hydrogen bond. Theophylline and orcinol molecules form infinite

chains running parallel to each other (Figure 2.A.7a). Similar chain connecting the imidazole molecule of theophylline (synthon E, Scheme 2.A.2) can be seen in the anhydrous form of theophylline molecule. The 3D packing of the cocrystal is fulfilled by the water molecule connecting the layers formed via Orc and theophylline chains (Figure 2.A.7b).
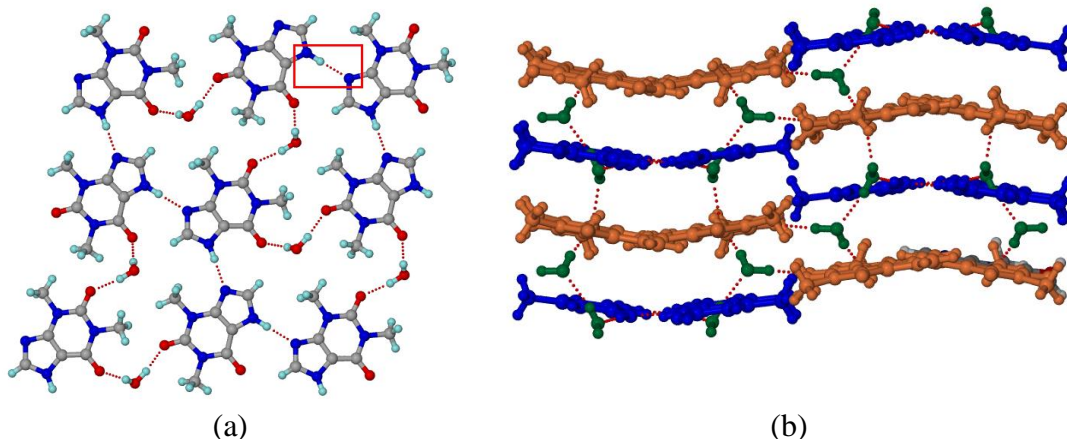

(a)   (b)

Figure 2.A.7 The theophylline molecules are arranged as catemeric N−H⋯N hydrogen bonds in cocrystal **3** similar in cocrystal **2**. (b) Water molecules act as hydrogen bonded connector of the 2D wavy molecular sheets formed by the API and coformer leading to 3D packing.

THP•2,6-DHBA•H₂O [**4**]: The 2,6-DHBA coformer resulted in a salt structure of theophylline with 1:1 stoichiometry. It is a monohydrate where the carboxylic proton is transferred to the imidazole *N* of theophylline molecule. The two hydroxyl groups of the 2,6-DHBA took part in an intramolecular hydrogen bond with the carboxylate oxygen atoms. Bučar et al. studied the involvement of intramolecular O−H$_{hydroxy}$⋯O$_{carboxyl}$ hydrogen bond for *ortho*-hydroxybenzoic acid on cocrystallizing with caffeine and inclusion of water molecule in the crystal structure [15]. Due to the intramolecular H-bond, the hydroxyl groups are unable to participate in intermolecular H-bonding. The water molecule connects the theophylline dimer through O−H⋯O and N−H⋯O hydrogen bond (Figure 2.A.8a). The theophylline-2,6-DHBA forms a layer along (0 1 0) plane and the water molecule connects the 2D layers through O−H⋯O hydrogen bond as shown in Figure 2.A.8a.

<center>(a)   (b)</center>
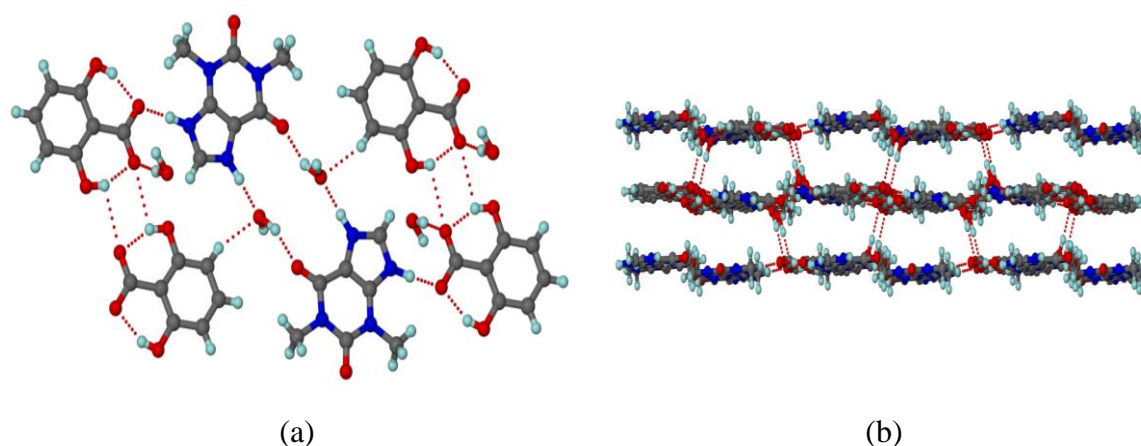
Figure 2.A.8 (a) The –COOH proton from 2,6-dihydroxybenzoic acid is transferred and sits on the basic N centre of the imidazole ring. The theophylline forms N−H···O dimer bridged by a water molecule in **4** [THP•2,6-DHBA•2H$_2$O]. Both –OH groups are engaged in intramolecular hydrogen bonding and water involves in assembling 2D layers of API and coformers into a 3D structure (b).

Theo•3,5-DHBA [**5**]: The crystal structure was solved in triclinic $P\bar{1}$ space group. Cocrystals of 1:1 stoichiometry of theophylline and 3,5-DHBA was crystallized out using a solvent mixture of CHCl$_3$ and MeOH in 4:1 ratio. The –COOH group forms hydrogen bond with the imidazole N atom similar to the reported cocrystals with the aliphatic dicarboxylic acids (synthon A, Figure 2.A.9a. Two theophylline molecule forms a dimer through N−H···O hydrogen bond between the *exo*-carbonyl O and imidazole N−H group similar to the monohydrate and the aliphatic dicarboxylic acid cocrystals. The second carbonyl group forms an O−H···O hydrogen bond with one of the hydroxyl groups of 3,5-DHBA. All the hydrogen bonding functional group are utilized in hydrogen bonding results a planar molecular sheet parallel to (2 1 -1) plane (Figure 2.A.9b).
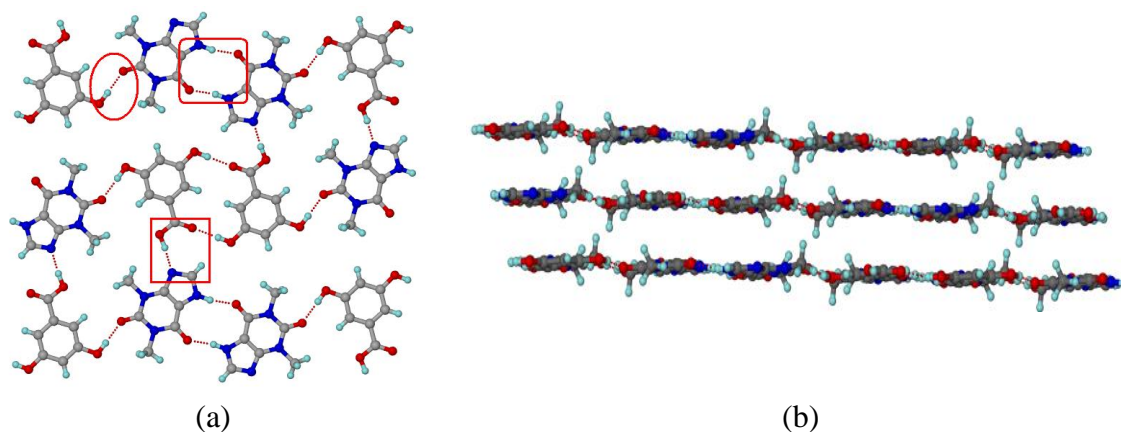
(a)   (b)

Figure 2.A.9 (a) Involvement of all functional groups in hydrogen bonding permits no water inclusion. Theophylline forms N−H···O dimers and one of the –OH groups and C=O from 3,5-dihydroxybenzoic acid form O−H···O dimers in cocrystal **5**. (b) 2D molecular layers are stacked via weak interactions like $\pi \cdots \pi$ and C−H$\cdots \pi$ that complete crystal structure.

THP•3,4-DHBA [**6**]: Single crystal data of **6** were solved and refined in triclinic $P\bar{1}$ space group. The common synthons **A**, **B** or **C** are found absent in the crystal structure (synthons are shown in Scheme 2.A.2). Rather, carboxylic acid group of 3,4-DHBA forms a homodimer with an adjacent molecule. The two hydroxyl group interact with the theophylline molecule, one with the imidazole N atom forming an O−H···N hydrogen bond and the other with endo-carbonyl via discrete (**D**) O−H···O hydrogen bond synthon (Figure 2.A.10a). Theophylline dimer synthon **D** is present in this cocrystal as well as similar to that of cocrystal **5**. Hydrogen-bonded theophylline-3,4-DHBA sheets stacked parallel to (-2 2 1) plane with the help of π-π interaction to fulfil the 3D packing (Figure 2.A.10b).
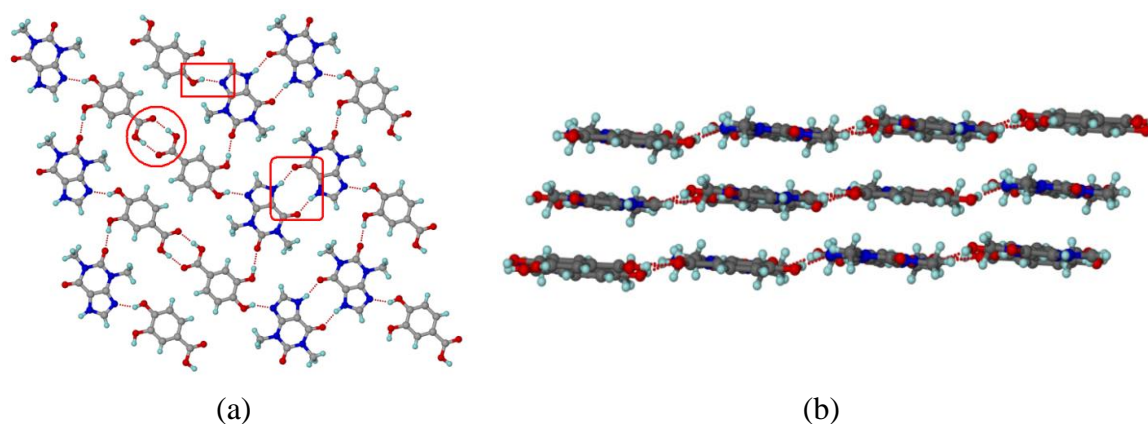

(a)   (b)

Figure 2.A.10 (a) Carboxylic acid homodimer is formed via O−H···O hydrogen bonds in addition to theophylline N−H···O dimers in cocrystal **6**. The two –OH groups were

engaged in hydrogen bonding to connect two API via N−H···O dimer that forms a 2D molecular sheet which further stacked through weak interaction into 3D packing (b).

THP•CA [**7**]: Needle-shaped crystals of theophylline and cinnamic acid cocrystals with 1:1 stoichiometry was obtained, solved and refined in monoclinic $P2_1/c$ space group. Unlike the theophylline-dicarboxylic acids cocrystals reported in the literature, cinnamic acid forms a carboxylic acid two-point synthon (synthon C) with *exo*-carbonyl O of pyrimidine ring, and the N−H hydrogen of the imidazole ring of theophylline (Figure 2.A.11a). Due to the presence of this strong N−H···O and O−H···O hydrogen bond synthon, hydrate formation is avoided. The discrete THP-CA dimers are connected via weak C−H···N interaction forming an infinite zigzag tape, stacked parallel to (1 0 -2) plane (Figure 2.A.11b) via π-π stacking.

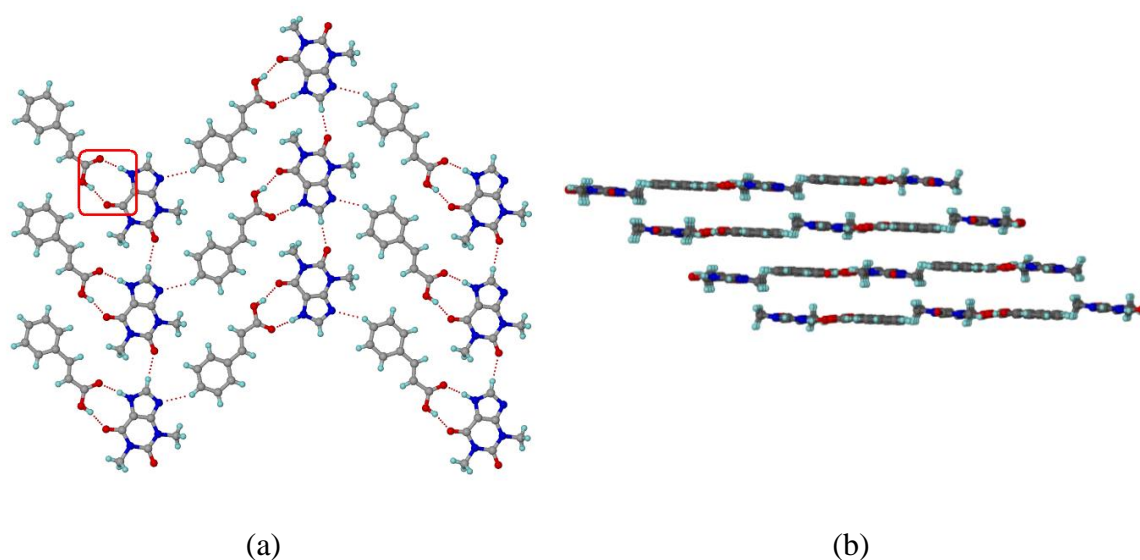(a)   (b)

Figure 2.A.11 (a) Carboxylic acid forms stronger two-point acid···amide like synthon via O−H···O and N−H···O hydrogen bonds in cocrystal **7**. The API···coformer units are further assisted by weak C−H···N and C−H···O hydrogen bonds leading to 1D zig-zag chains. (b) The 2D molecular layers are stacked by weak interactions completes the 3D arrangement of molecules in the lattice.

Table 2.A.4 Hydrogen bond matrices for cocrystal **1**-**7** with symmetry codes

Cocrystals	Interaction	H···A/ Å	D···A/ Å	∠D–H···A/º	Symmetry code
1 [THP•Res•H₂O]	O₃–H₃···O₁	1.75	2.680(2)	156	-1/2+x,-1/2+y,z
	O₄–H₄···O₅	1.72	2.697(2)	174	-
	N₄–H₄A···O₅	2.28	3.024(2)	130	x,1-y,-1/2+z
	N₄–H₄A···O₃	2.10	2.862(2)	131	1/2+x,1/2+y,z
	O₅–H₅A···O₂	1.83	2.777(2)	162	x,1+y,z
	O₅–H₅B···N₃	1.94	2.918(2)	175	1/2+x,1/2-

					y,1/2+z
	C_1–H_1···O_1	2.47	3.345(2)	137	-1/2+x,1/2-y,-1/2+z
	C_{11}–H_{11}···O_4	2.42	3.497(2)	173	-1/2+x,1/2-y,-1/2+z
2 [THP•Phu•H₂O]	N_2–H_2···N_1	1.76	2.764(2)	180	x,1/2-y,1/2+z
	O_3–H_3···O_2	1.76	2.747(2)	178	1-x,-y,-z
	O_4–H_{4A}···O_6	1.66	2.640(2)	173	x,y,-1+z
	O_5–H_5···O_4	1.74	2.720(2)	172	x,1/2-y,1/2+z
	O_6–H_{6D}···O_5	1.85	2.809(2)	165	-
	O_6–H_{6E}···O1	1.85	2.797(2)	160	-
	C_1–H_1···O_1	2.42	3.321(2)	139	x,1/2-y,-1/2+z
3 [THP•Orc•2H₂O]	N_1–H_2···N_2	1.84	2.847(4)	172	-1/2+x,y,1/2-z
	O_3–H_3···O_6	1.65	2.628(4)	175	-1+x,y,z
	O_4–H_4···O_3	1.79	2.768(4)	173	1/2+x,y,1/2-z
	O_5–H_{5A}···O_2	1.81	2.781(4)	171	1/2+x,1/2-y,-z
	O_5–H_{5B}···O_1	1.84	2.813(3)	168	1+x,y,z
	O_6–H_{6D}···O_5	1.84	2.753(5)	152	-
	O_6–H_{6E}···O_1	2.29	3.008(4)	129	1/2-x,1/2+y,z
	C_1–H_1···O_1	2.44	3.218(4)	128	1/2+x,y,1/2-z
4 [THP•2,6-DHBA•H₂O]	N_3–H_3···O_3	1.59	2.600(1)	177	x, 3/2-y,1/2+z
	N_4–H_4···O_7	1.67	2.678(2)	175	-x,1/2+y,1/2-z
	O_7–H_{7D}···O_1	1.92	2.848(2)	157	x,3/2-y,1/2+z
	O_7–H_7E···O_4	1.87	2.845(2)	173	x,1/2-y,1/2+z
	C_1–H_1···O_5	2.13	3.205(2)	175	-x,1/2+y,1/2-z
	C_6–H_{6A}···O_3	2.28	3.351(2)	169	x,3/2-y,1/2+z
	C_{11}–H_{11}···O_7	2.41	3.441(2)	158	-
	C_{13}–H_{13}···O_2	2.36	3.419(2)	165	1-x,-1/2+y,1/2-z
5 [THP•3,5-DHBA]	N_2–H_2···O_1	1.74	2.734(1)	169	1-x,1-y,-z
	O_4–H_4···N_1	1.74	2.715(1)	174	-1+x,1+y,z
	O_5–H_5···O_2	1.75	2.734(1)	175	1-x,1-y,1-z
	O_6–H_6···O_3	1.82	2.799(1)	171	-x,1-y,-z
	C_1–H_1···O_6	2.37	3.442(2)	170	1-x,-y,-z
	C_{10}–H_{10}···O_2	2.44	3.221(1)	128	1-x,1-y,1-z
6 [THP•3,4-DHBA]	O_3–H_3···O_4	1.66	2.639(2)	177	1-x,2-y,-z
	N_4–H_4···O_1	1.78	2.764(2)	165	1-x,1-y,-z
	O_5–H_5···O_2	1.72	2.701(2)	179	2-x,2-y,1-z
	O_6–H_6···N_3	1.87	2.746(2)	148	1-x,1-y,1-z
	C_7–H_{7A}···O_6	2.30	3.234(2)	143	1-x,1-y,1-z
	C_7–H_{7C}···O_5	2.38	3.421(2)	161	1+x,y,z
7 [THP•CA]	N_2–H_2···O_4	1.76	2.761(2)	169	1-x,2-y,-z
	O_3–H_3···O_1	1.69	2.644(2)	164	1-x,2-y,-z
	C_1–H_1···O_2	2.11	3.186(2)	175	x,1+y,z
	C_7–H_{7B}···N_1	2.53	3.453(2)	143	2-x,-1/2+y,1/2-z

2.A.3.3 Physical Stability

Being aware of the instability of theophylline towards humidity, we decided to perform a stability test for the cocrystal materials towards high relative humidity (RH). Accordingly, an experiment of continuous unit cell parameter checking has been performed by keeping the crystals at RH 90%. Unit cell were determined at specific intervals over a time span of 3 months. Cocrystals **1**, **3**, **5**, **6** and **7** are considered for this measurement. A suitable single crystal from each system is subjected to the experiment. Same crystal was kept for one day at RH 90% and determined the cell parameter again. The experiment was repeated for the crystal after 7 days and 90 days. This stability test was performed in order to examine whether the synthesized cocrystals offer enhanced physical stability towards high moisture environment. It is already reported by many groups that at the high humid and/ or aqueous conditions theophylline transform to the monohydrate form. Interestingly, we have observed consistency of cell parameter over the time window of 3 months at 90% RH for the cocrystals **5**, **6** and **7** (Table 2.A.5 includes unit cell parameter of cocrystal **5** & **6**). However, the release/ reuptake of water molecules from the crystalline lattice of **1** and **3** disrupt crystallinity. Thus it was not possible to perform the experiment afterwards. PXRD patterns of the cocrystal materials preserving at different RH and recorded at a time to time and then evaluating weight loss in, thermogravimetric analysis etc. predict the hydration profile of each sample.

To shed light into water-mediated cocrystal transformation into its starting materials or a hydrate of them, we further investigated the qualitative (and quantitative) study on hydration profile for cocrystal **1**. Bulk sample is kept at 90% RH and PXRD was evaluated over time to time. The powder pattern recorded after 3 days the arrival of a few new peaks at 2θ 8.82, 11.64, 14.90, 27.51, 35.01 etc. All new peaks get better with intensity over time (at 7 days and so on) and they refer to the monohydrate of drug theophylline (Figure 2.A.12)

Table 2.A.5. Unit cell parameter determination of cocrystals at 90 RH %, over a time span of 90 days to understand the physical stability. Cocrystals 1, 3, 5, 6, and 7 were subjected for this test and found that 5, 6 are stable demonstrated from identical cell parameter even after 90 days.

| Unit cell	THP•3,5-DHBA [5]			THP•CA [6]		
Time	RH 90% 1 day	RH 90% 7 days	RH 90% 90 days	RH 90% 1 day	RH 90% 7 days	RH 90% 90 days
Crystal system	Triclinic	Triclinic	Triclinic	Triclinic	Triclinic	Triclinic
T [K]	296	296	296	296	296	296
a [Å]	7.3335 (2)	7.3191 (4)	7.2998 (2)	8.0967 (4)	8.1252 (6)	7.9940 (5)
b [Å]	8.0398 (2)	8.0348 (3)	8.0468 (2)	8.6123 (4)	8.6098 (5)	8.5845 (5)
c [Å]	12.6932 (2)	12.6490 (4)	12.7015 (2)	11.5921 (4)	11.5901 (5)	11.6891 (5)
α [°]	81.6945 (9)	82.0012(9)	81.6640 (7)	103.170 (3)	102.968 (3)	102.892 (3)
β [°]	85.6101 (9)	85.5321 (8)	85.5910 (9)	104.986 (4)	104.963 (6)	105.293 (5)
γ [°]	82.1699 (9)	82.2003 (8)	82.1648 (9)	105.098 (3)	105.762 (4)	105.440 (4)
Volume [Å^3]	729.44 (3)	738.34 (3)	735.67 (4)	721.82 (9)	717.76 (10)	719.23 (10)
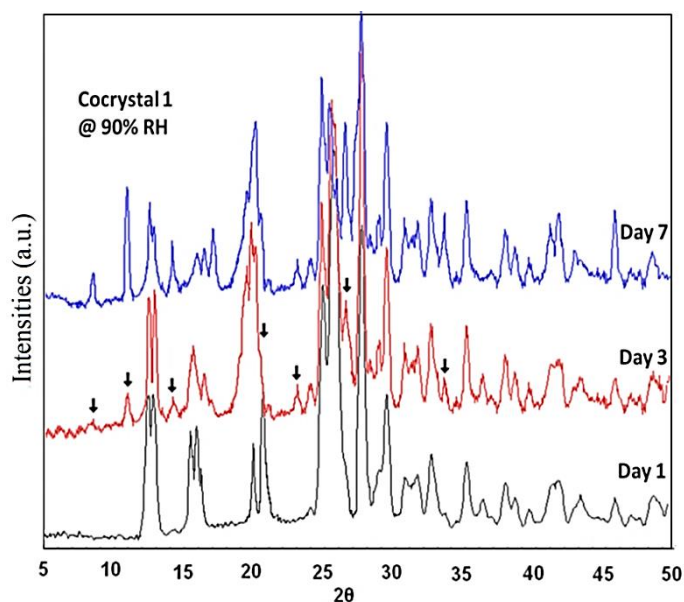
Figure 2.A.12 PXRD patterns of a bulk sample of cocrystal **1** kept at relative humidity 90% show water-mediated transformation into monohydrate of theophylline and the resorcinol. The arrival of new peaks after 3 days marked (pattern in red) is the indication of decomposition of cocrystal into its coformers and/or coformer hydrate.

2.A.3.4 Solubility Determination

The aqueous solubility of all the cocrystal materials is evaluated by using UV-Vis spectroscopy. Methods are described in the experimental section. All the cocrystals materials containing phenolic coformers show improved aqueous solubility compared to the parent drug theophylline. The obtained solubility parameters show that the cocrystal **3** (34.50 mg/mL) has over two-fold aqueous solubility than the drug theophylline. The cocrystal **1** (23.6 mg/mL) and **2** (27.20 mg/mL) also displays the similar trend. Aqueous solubility for cocrystal **4** is found to be 17.60 mg/mL which is considerably higher than that of independent coformer 2,6-dihydroxybenzoic acid i.e. 2.50 mg/mL. The higher solubility can be attributed from the formation of weaker O−H⋯O intermolecular H−bonding. In addition cocrystal **4** is ionic in nature. The dissociation of cocrystals in aqueous solution is commonly known to happen for many cocrystal systems that include a drug known to form hydrates. An important observation from the single crystal structures of hydrated crystals is that the water molecule plays a key role in bridging drug⋯drug and drug⋯coformer interaction. This, in turn, lowered the stability of these cocrystals and dissociate to its coformer and API. On the contrary, the non-hydrated cocrystals show considerably lower aqueous solubility because of the presence of stronger intermolecular COOH⋯N$_{imidazole}$ H-bonding. Cocrystal **5** shows negligible aqueous solubility (0.14 mg/mL). In this cocrystal, all the functional groups are involved in forming stronger hydrogen bond interactions. This minimises the possibility of more solute⋯solvent interactions, thus shows less solubility. Cocrystal **6** exhibits considerable aqueous solubility i. e. 12.4 mg/mL. The coformer 3,4-DHBA is involved in carboxylic acid homodimer formation via O−H⋯O hydrogen bonds thereby leaving only the –OH groups for weak intermolecular H−bonding with the API molecules. The cocrystal **7** falls into the same trend showing only 0.62 mg/mL aqueous solubility. The solubility of theophylline is measured and found 8.24 mg/mL at 20 °C (Literature value 8.3 mg/mL) and compared with the cocrystals solubilities as shown in Figure 2.A.13. The dissimilarity in solubilities of the cocrystal materials is further correlated with the different hydrogen bond synthon involved in the cocrystal formation and their energies in the following section.
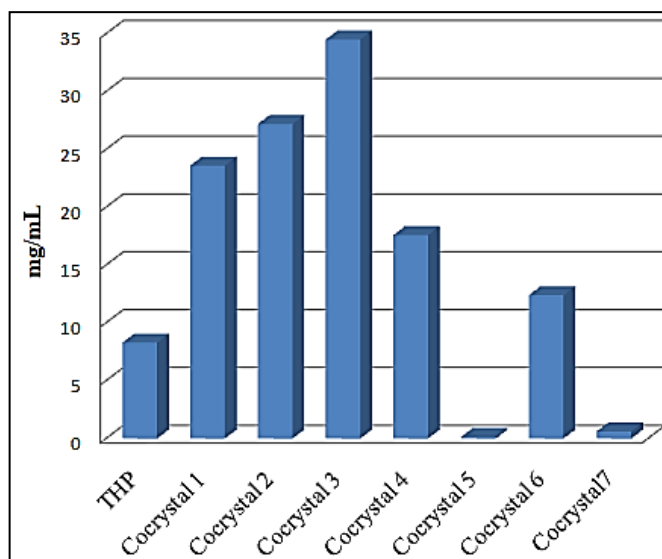
Figure 2.A.13 Aqueous solubility comparison of drug THP and the cocrystals.

2.A.3.5 Hydrogen bond synthon and CSD analysis

Hydrogen bonding and synthon competition among the cocrystals were accessed in terms of their synthon energy and analysed with Mercury 3.9. Cambridge Structural Database (CSD) search with "theophylline" fragment is carried out with 3D coordinates, restricted to organic molecules only. ConQuest 1.19, CSD version 5.38, Nov 2017 Updates, www.ccdc.cam.ac.ukupdate is used in all searches and crystal structures were visualized in Mercury 3.9. The lower R-factor structure is retained for duplicate refcodes. The search results total 59 hits.

These structures were manually filtered to 59 crystal structures of which theophylline cocrystallized with aromatic carboxylic acids (43 hits), aliphatic carboxylic acids (11 hits) and with phenolic compounds (5 hits) and listed in Table 2.A.6. None of the structure is found ionic except WUYRUD where the proton transfer has occurred from the $-SO_3H$ group. All the theophylline cocrystals with COOH groups were subdivided into three categories based on the supramolecular synthon present (Scheme 2.A.2). Out of the 59 cocrystals, 16 cocrystals contain imidazole-carboxylic acid two-point synthon A (27 %), 8 of them having imidazole-carboxylic acid one-point synthon B (13%), whereas 14 cocrystals consist of carboxylic acid two-point synthon C, connecting *exo*-O of pyrimidine ring and imidazole N−H (23 %). Higher probability of synthon A is due to the formation of stronger hydrogen bond between imidazole and carboxylic acid group. Synthon C behaves like strong acid···amide like heterosynthon.
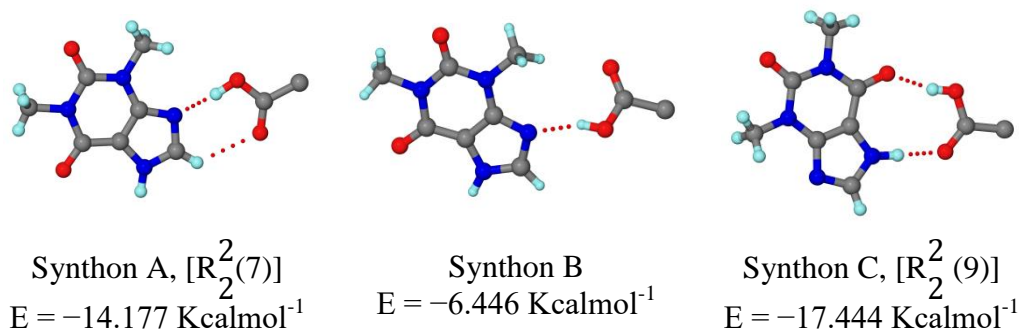
Table 2.A.6 Hydrogen bond synthon of theophylline cocrystals compared with CSD. Coformers selected as aromatic and aliphatic carboxylic acids and phenols. Synthon A and C refer to 2.A.2 are found quite common in crystal structures. Presence of –OH groups facilitate the formation of N−H⋯O homo dimmers of the API theophylline.
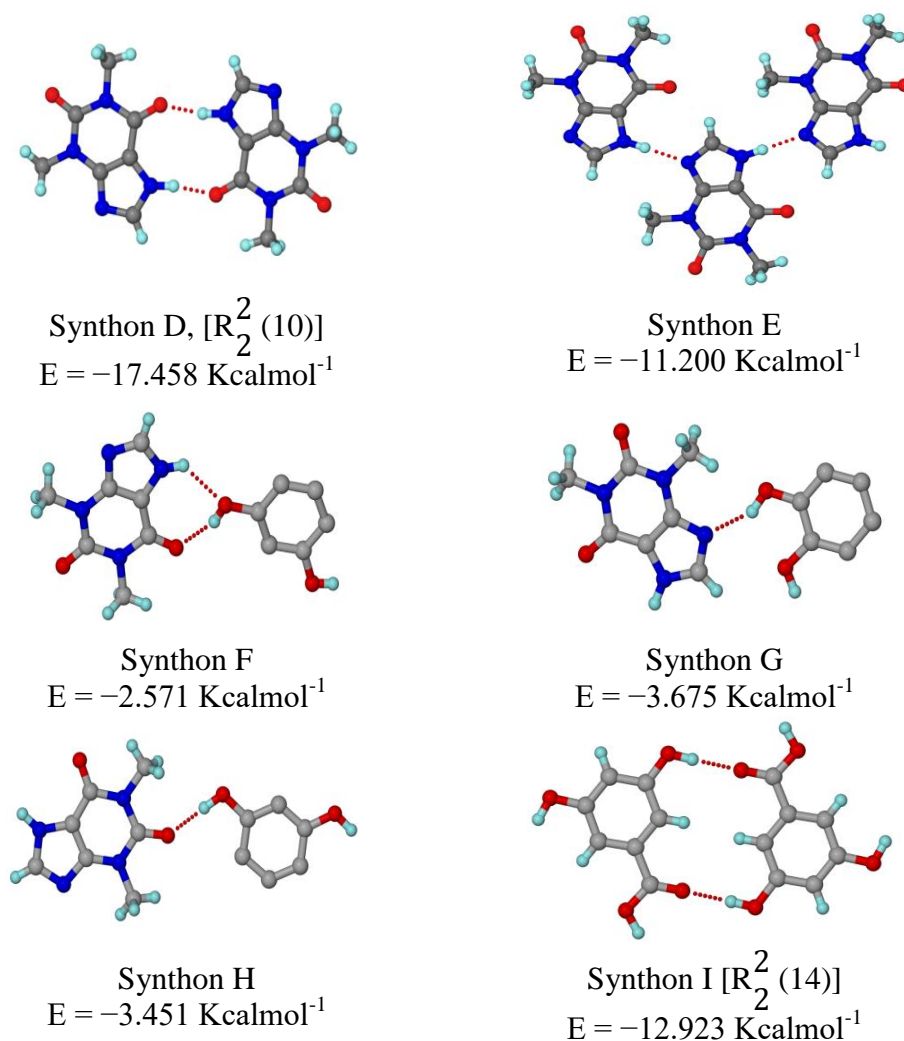
Aromatic –COOH group		Aromatic –COOH group		Aliphatic –COOH group		–OH group	
Refcode	Synthon	Refcode	Synthon	Refcode	Synthon	Refcode	Synthon
LEDVOH	E	OPULUI	D	CIZTAH	A	GAFTUE	D, G, H
VAXSAQ	C	OPUMAP	D	CODCOO	A	KIGLUI	D
CSATEO	A, D	OPUMAP01	-	KIGKAN	-	KIGLUI01	D
DEYREF	C	OPUMUJ	B, D	KIGLAO	C	HEBFEB	D, H
DUCROJ	A, D	OPUNAQ	C	NEXWOD	B	HEBFIF	D, H
IJIBEJ	C, H	OPUNEU	A, C	NEYCIE	B, D		
IJIBEJ01	C, G	OPUNIY	D	WUYROX	-		
KIGLES	A, D	YEVNIZ	B, D	XEJWUF	B, D		
KIGLIW	A, D	YUJLOG	D	XEJXAM	A, D		
KIGLOC	C, G	YUJLOG01	D	XEJXEQ	A, D		
LUKXUL	A, C	ZEKPIR	B, D	XEJXIU	A, D		
UNITER	A, C	ZEKPIR01	D				
UNITIV	A	ZIQDUA	-				
HUMNEK	-	ZOYBIA	C				
OPUKIV	A, D	WUTJAY	C				
OPUKOB	D	WUTHOK	D				
OPUKUH	D	WUTHUQ	D				
OPUKUH01	C	WUTHIE	A, D				
OPULES	B, D	WUTHEA	D				
OPULES01	-	WUYRUD	-				
OPULOC	D						
OPUMOD	C						
OPUNOE	A, D		-				

Hydrogen bond synthon [presented in Scheme 2.A.2] energies are calculated with Gaussian 09 (B3LYP/6-31G* (d,p). The COOH⋯$N_{imidazole}$ two-point interaction in synthon A and C are found stronger than single point synthon B. A high occurrence of synthon A and C in reported structures also supported the same. Setting up stronger interaction between API and coformers would certainly predict better physical stability of that cocrystal. Another interesting observation is that the aliphatic and aromatic acids with lower pK_a (< 4) prefer synthon A and B; whereas acids with moderate pK_a (≥ 4) and having hydrogen bond donor functionality at *m/p* position (aromatic acid) results synthon C. The competition between the carboxylic acid two-point heterosynthon A and acid-triazole synthon B is compared with CSD database and correlated with pK_a of carboxylic acids. Stronger acids prefer synthon B and moderate to weak acids resulted formation of

synthon A. The N−H···O dimer synthon D is formed as secondary synthon while synthon A is present. An absence of –COOH group and/or presence of –OH group normally lead to synthon D. Catemeric N−H···O formed by theophylline is not generally found except in LEDVOH and cocrystal **3** in this study. The large pK_a difference of 2,6-DHBA ($pK_a = 1.26$) and theophylline ($pK_a = 8.6$) led to proton transfer.

Presence of hydroxyl group in the molecule and especially their position in hydroxybenzoic acids plays the key role in solvent inclusion. As reported in the literature cocrystal of theophylline with 2,4-DHBA, caffeine with 3,5-DHBA and theophylline with 2,6-DHBA (present study) are hydrate structure, whereas, coformer like *p*-hydroxybenzoic acid, gentisic acid produce anhydrous cocrystals [25]. In the cocrystal structure of theophylline studied here show neutral conformation except the purine *N* is protonated in cocrystal **4**. The position of OH groups in isomeric dihydroxybenzoic acids plays an important role in the inclusion of crystallizing media into the crystal lattice. Carboxylic acid homodimer formation in their solvated crystal structures was commonly observed except in dioxane solvate and guest free melt polymorph structures. The two OH groups of 3,5-DHBA can adopt 4 possible conformations and the *anti-anti* conformation is present in cocrystal **5**. The uncommon *anti-anti* conformation of two hydroxyl groups of 3,5-DHBA is also observed in the guest free melt polymorph 3,5-DHBA (refcode WUYPOW) and cocrystal with caffeine (MOZCEK). The 3,4-DHBA forms a carboxylic acid homodimer in cocrystal **6** but the acid dimer synthon is absent in cocrystals **4** and **5**.

Synthon A, [$R_2^2(7)$]
E = −14.177 Kcalmol^{-1}

Synthon B
E = −6.446 Kcalmol^{-1}

Synthon C, [$R_2^2(9)$]
E = −17.444 Kcalmol^{-1}

Synthon D, [R$_2^2$ (10)]
E = −17.458 Kcalmol^{-1}

Synthon E
E = −11.200 Kcalmol^{-1}

Synthon F
E = −2.571 Kcalmol^{-1}

Synthon G
E = −3.675 Kcalmol^{-1}

Synthon H
E = −3.451 Kcalmol^{-1}

Synthon I [R$_2^2$ (14)]
E = −12.923 Kcalmol^{-1}

Scheme 2.A.2 Assorted hydrogen bonded synthons that are observed in the crystal structures of 1-7 between API theophylline and coformer functional groups such as –COOH and –OH. Two point theophylline N−H···O dimer (synthon D) and single point catemer synthon assisted by weak C−H···O (synthon E), two-point (synthon A), single point (synthon B) −COOH···NH$_{imidazole}$ hydrogen bonds, and synthon C are assessed in terms of their stabilization energy which could translate into the physical stability of cocrystals. Synthon energies were calculated on DFT using Gaussian03 and B3LYP; 6311G*(d,p) as basis set.

2.A.4 Summary

Poor moisture stability of many drugs creates frequent trouble in pharmaceutical industries. This study deals with strategic physical property modulation of cocrystals of drug theophylline synthesized using liquid assisted mechanochemical grinding. Two sets of coformers belonging to phenol and isomeric dihydroxybenzoic acid are chosen, as they are known to form weaker and stronger hydrogen bond in cocrystals. Aqueous

solubility and hydration stability of the cocrystals are evaluated. Synthon energy calculation using DFT is performed for all the hydrogen bond synthons observed in the cocrystals. The synthon energies are further correlated with the properties of cocrystals. Though extensive hydrogen bonding exists within the structures, it is observed that the phenols are not suitable coformers to prevent hydration of theophylline cocrystals. This, in fact, is reflected in low moisture stability and high aqueous solubility of cocrystals with phenolic coformers. Additionally, we observed that the presence of weaker H bond and unmatched donor-acceptor ratios facilitate water assimilation into the crystal lattice for cocrystal having phenolic coformers. Indeed the weaker $-OH \cdots N_{imidazole}$, $-OH \cdots O$ promote incorporation of crystalline water which instigated higher aqueous solubility and very low moisture stability. However hydroxybenzoic acids are found to be a better choice to provide extra stability to the API. The stronger $-COOH \cdots N_{imidazole}$ heterosynthon presence is found responsible for the enhanced stability of the cocrystals. Likewise, a sharp decrease in solubility for cocrystals with isomeric hydroxybenzoic acids is observed and correlated with the existence of stronger hydrogen bonds. Such studies will surely aid the formulation scientists in the pharmaceutical industry to develop a new solid formulation of a drug.

2.A.5   Experimental Section

2.A.5.1 Materials

Theophylline and coformers listed in Scheme 2.A.1 were purchased from Sigma Aldrich and used as received without further purification. The analytical-grade solvents used for the studies are obtained from Merck and used without further purification.

2.A.5.2 Preparation of cocrystals

Solvent-assisted mechanochemical grinding is used to prepare all the cocrystals. An equivalent amount of theophylline and each coformer were individually taken in a mortar and ground with a pestle for around ~45 minutes with dropwise addition of CH_3CN. The mixture was then transferred into a vial and dissolved in a 1:4 mixture of CH_3OH and $CHCl_3$ with ~50 °C warm condition. The solution is kept undisturbed and allowed for cocrystallization at room temperature with slow evaporation. Suitable crystals for single crystal data collection obtained within in 2-3 days. Rod and needle-shaped crystals were

grown for the cocrystal of Theophylline with Orc and CA otherwise block transparent crystals were common for the rest. Crystals were then subjected for spectroscopic, thermal and X-ray diffraction analysis. The drug:coformer ratio in cocrystals **1** to **7** are found in 1:1. With phenolic coformers by slow evaporation of solution are found inefficient cocrystal synthesis and therefore rigorous grinding is necessary to give the product cocrystals. Mechanochemical synthesis or cogrinding are known to be the classical methods to prepare molecular complexes that promote the formation of microcrystalline seeds of the cocrystals in the solution to grow single crystals for X-ray diffraction [30,31]. Indeed, we realized such liquid-assisted grinding as a powerful methodology to construct cocrystals in a rapid and quantitative manner.

2.A.5.3 Vibrational Spectroscopy

A Nicolet 6700 FT-IR spectrometer with a NXR FT-Raman Module was used to record IR spectra. IR spectra were recorded on samples dispersed in a KBr pellet. All major stretching vibrations for cocrystals 1-7 are; THP·RES·H_2O (1): 3465 (O−H), 3292 (NH), 1683 (C=O, C=N), 1521 (C=C, C=O), 1329 (C−N), 1282 (C−N, w), 1220 (C−N), 863 (N−C−H) cm^{-1}; THP·PHU·H_2O (2): 3431(OH), 3261 (N−H), 1692 (C=O, C=N), 1571 (C=O), 1329 (C−N), 1294 (C−O), 832 (N−C−H) cm^{-1}; THP·ORC·$2H_2O$ (3): 3472 (OH), 1693 (C=O, C=N), 1341 (C−N), 863 (N−C−H) cm^{-1}; THP·2,6-DHBA·H_2O (4): 3345 (O−H), 3137 (N−H), 1698 (C=O, C=N), 1560 (COO$^-$), 1404 (COO$^-$), 1328 (C−N), 1302 (C−O), 1220 (C−N), 884 (N−C−H) cm^{-1}; THP·3,5-DHBA (5): 3431 (O−H), 3277 (N−H), 1685 (C=O, C=N), 1559 (C=O), 1353 (C−N), 1330 (C−O), 1256 (C−N), 855 (N−C−H) cm^{-1}; THP·3,4-DHBA (6): 3460 (O−H), 3108 (N−H), 1684 (C=O, C=N), 1348 (C−N), 1292 (C−O), 1220 (C−N), 859 (N−C−H) cm^{-1}; THP·CA (7): 3460 (O−H), 3098 (N−H), 1700 (C=O, C=N), 1560 (C=O), 1328 (C−N), 1283 (C−O), 1220 (C−N), 863 (N−C−H) cm^{-1}.

2.A.5.4 Powder X-ray diffraction

Powder XRD of all samples was recorded on a PANlytical 1830 (Philips Analytical) diffractometer using Cu-Kα X-radiation (λ = 1.54056 Å) at 35 kV and 25 mA. Diffraction patterns were collected over a 2θ range of 5-50° at a scan rate of 5° min^{-1}. The Powder Cell 2.3 program was used for Rietveld refinement.

2.A.5.5 Thermal Analysis

DSC and TGA were performed on a Mettler Toledo DSC 822e module and a Mettler Toledo TGA/SDTA 851e module, respectively. Samples were placed in open alumina pans for TGA and in crimped but vented aluminium sample pans for DSC. The typical sample size is 4-6 mg for DSC and 9-12 mg for TGA. The temperature range was 30-300 °C at 2 Kmin^{-1} for DSC and 10 Kmin^{-1} for TGA. Samples were purged with a stream of dry N2 flowing at 150 mL min^{-1} for DSC and 50 mL min^{-1} for TGA.

2.A.5.6 Single Crystal X-ray Diffraction

X-ray reflections were collected on a Bruker SMART CCD diffractometer using Mo Kα (λ =0.71073 Å) radiation. Data reduction was performed using Bruker SAINT Software [37]. Intensities for absorption were corrected using SADABS. Structures were solved and refined using SHELXL-2008 with anisotropic displacement parameters for non-H atoms [38]. Hydrogen atoms on O and N were experimentally located in all crystal structures. All C-H atoms were fixed geometrically using the HFIX command in SHELX-TL. X-Seed was used to prepare figures and packing diagrams [39]. A check of the final CIF file using PLATON did not show any missed symmetry [40,41]. The crystallographic parameters for all structures are summarized in Appendix Table A.1. The hydrogen bond distances in the X-ray crystal structures (Table 2.A.4) are neutron-normalized by fixing the D-H distance to its accurate neutron value (O-H 0.983 Å, N-H 1.009 Å, C-H 1.083 Å).

2.A.5.7 DFT Computations

Hydrogen bond synthon energies were calculated with Gaussian03 (B3LYP/6-31G* (d,p). Observed conformations and orientations of molecules in the crystal structure considered for the energy calculation without further optimization to the gas phase minimized conformers.

2.A.5.8 Solubility Determination

A series of standard solution (i.e. concentration 0.1 mmol, 0.2 mmol, 0.3 mmol, 0.4 mmol etc.) of cocrystals were prepared in water to construct absorbance versus concentration calibration curve for each cocrystal material. The experiment was run for

triplicate for consistency. An excess amount of each cocrystal was added individually to 20 mL of water in a jacketed, circulating flask maintained at 25 °C. Cocrystals (**1**, **2** & **3**) with phenol coformers and **4**, **5**, & **6** with isomeric hydroxybenzoic acid coformers and 7 with cinnamic acid were considered for aqueous solubility study using UV-Vis spectrometry. The suspension was kept for overnight stirring. After filtering through a syringe filter of 0.45 μm size, the absorbance was determined by measuring the ultraviolet (UV) absorption at 270 nm. All experiments were performed in HALO DB-30 UV−Visible double beam spectrophotometer. The experiment for unknown concentration solution was also repeated for three times. The concentration of the unknown solution (C_u) of the cocrystal was evaluated from the slope and intercept of the calibration curve by using the formula C_u = (A_u-Intercept)/Slope, where A_u is the absorbance of the unknown solution. To compare solubility data extracted from UV-Vis calibration curves we again performed gravimetric measurement for solubility determination. A fixed volume (2 mL) of an individual sample was taken at a regular interval, and the concentration was determined gravimetrically with a good agreement measured by UV-Vis.

2.A.6 References

[1] Walsh, R. B., Bradner, M. W., Fleischman, S., Morales, L. A., Moulton, B., Rodriguez-Hornedo, N., and Zaworotko, M. J. Crystal engineering of the composition of pharmaceutical phases. *Chemical Communications*, 9(2):186-187, 2003.

[2] Remenar, J. F., Morissette, S. L., Peterson, M. L., Moulton, B., MacPhee, J. M., Guzmán, H. R., and Almarsson, Ö. Crystal engineering of novel cocrystals of a triazole drug with 1,4-dicarboxylic acids. *Journal of the American Chemical Society*, 125(28):8456-8457, 2003.

[3] Almarsson, Ö. and Zaworotko, M. J. Crystal engineering of the composition of pharmaceutical phases. Do pharmaceutical co-crystals represent a new path to improved medicines? *Chemical Communications*, (17):1889-1896, 2004.

[4] Schultheiss, N. and Newman, A. Pharmaceutical cocrystals and their physicochemical properties. *Crystal Growth and Design*, 9(6):2950-2967, 2009.

[5] Good, D. J. and Naír, R. H. Solubility advantage of pharmaceutical cocrystals. *Crystal Growth and Design*, 9(5):2252-2264, 2009.

[6] Babu, N. J. and Nangia, A. Solubility Advantage of Amorphous Drugs and Pharmaceutical Cocrystals. *Crystal Growth & Design*, 11(7):2662-2679, 2011.

[7] Duggirala, N. K., Perry, M. L., Almarsson, Ö., and Zaworotko, M. J. Pharmaceutical cocrystals: Along the path to improved medicines. *Chemical Communications*, 52(4):640-655, 2016.

[8] Bolla, G. and Nangia, A. Pharmaceutical cocrystals: walking the talk. *Chemical Communications*, 52(54):8342-8360, 2016.

[9] Berry, D. J. and Steed, J. W. Pharmaceutical cocrystals, salts and multicomponent systems; intermolecular interactions and property based design. *Advanced Drug Delivery Reviews*, 117:3-24, 2017.

[10] Aakeröy, C. B. and Salmon, D. J. Building co-crystals with molecular sense and

supramolecular sensibility. *CrystEngComm*, 7(72):439-448, 2005.

[11]   Bhatt, P. M., Ravindra, N. V., Banerjee, R., and Desiraju, G. R. Saccharin as a salt former. Enhanced solubilities of saccharinates of active pharmaceutical ingredients. *Chemical Communications*, (8):1073-1075, 2005.

[12]   McNamara, D.P., Childs, S. L., Giordano, J., Iarriccio, A., Cassidy, J., Shet, M. S., Mannion, R., O'donnell, E., and Park, A. Use of a Glutaric Acid Cocrystal to Improve Oral Bioavailability of a Low Solubility API. *Pharmaceutical Research*, 23(8):1888-1897, 2006.

[13]   Du, M., Zhang, Z.-H., Zhao, X.-J., and Cai, H. Synthons Competition/Prediction in Cocrystallization of Flexible Dicarboxylic Acids with Bent Dipyridines. *Crystal Growth & Design*, 6(1):114-121, 2006.

[14]   Sarma, B., Nath, N. K., Bhogala, B. R., and Nangia, A. Synthon Competition and Cooperation in Molecular Salts of Hydroxybenzoic Acids and Aminopyridines. *Crystal Growth & Design*, 9(3):1546-1557, 2009.

[15]   Bučar, D. K., Henry, R. F., Lou, X., Duerst, R. W., MacGillivray, L. R., and Zhang, G. G. Z. Cocrystals of caffeine and hydroxybenzoic acids composed of multiple supramolecular heterosynthons: Screening via solution-mediated phase transformation and structural characterization. *Crystal Growth and Design*, 9(4):1932-1943, 2009.

[16]   Bethune, S. J., Huang, N., Jayasankar, A., and Rodríguez-Hornedo, N. Understanding and Predicting the Effect of Cocrystal Components and pH on Cocrystal Solubility. *Crystal Growth & Design*, 9(9):3976-3988, 2009.

[17]   Habgood, M. and Price, S. L. Isomers, conformers, and cocrystal stoichiometry: Insights from the crystal energy landscapes of caffeine with the hydroxybenzoic acids. *Crystal Growth and Design*, 10(7):3263-3272, 2010.

[18]   André, V., Fernandes, A., Santos, P. P., and Duarte, M. T. On the Track of New Multicomponent Gabapentin Crystal Forms: Synthon Competition and pH Stability. *Crystal Growth & Design*, 11(6):2325-2334, 2011.

[19]   Cheney, M. L., Weyna, D. R., Shan, N., Hanna, M., Wojtas, L., and Zaworotko, M. J. Coformer Selection in Pharmaceutical Cocrystal Development: a Case Study of a Meloxicam Aspirin Cocrystal That Exhibits Enhanced Solubility and Pharmacokinetics. *Journal of Pharmaceutical Sciences*, 100(6):2172-2181, 2011.

[20]   Jayasankar, A., Good, D. J., and Rodríguez-Hornedo, N. Mechanisms by which moisture generates cocrystals. *Molecular Pharmaceutics*, 4(3):360-372, 2007.

[21]   Trask, A. V. An overview of pharmaceutical cocrystals as intellectual property. *Molecular Pharmaceutics*, 4(3):301-309, 2007.

[22]   Cassidy, A. M. C., Gardner, C. E., and Jones, W. Following the surface response of caffeine cocrystals to controlled humidity storage by atomic force microscopy. *International Journal of Pharmaceutics*, 379(1):59-66, 2009.

[23]   Clarke, H. D., Arora, K. K., Bass, H., Kavuru, P., Ong, T. T., Pujari, T., Wojtas, L., and Zaworotko, M. J. Structure−Stability Relationships in Cocrystal Hydrates: Does the Promiscuity of Water Make Crystalline Hydrates the Nemesis of Crystal Engineering? *Crystal Growth & Design*, 10(5):2152-2167, 2010.

[24]   Jayasankar, A., Roy, L., and Rodríguez-Hornedo, N. Transformation Pathways of Cocrystal Hydrates When Coformer Modulates Water Activity. *Journal of Pharmaceutical Sciences*, 99(9):3977-3985, 2010.

[25]   Infantes, L., Fábián, L., and Motherwell, W. D. S. Organic crystal hydrates: What are the important factors for formation. *CrystEngComm*, 9(1):65-71, 2007.

[26]   Sarma, B. and Saikia, B. Hydrogen bond synthon competition in the stabilization of theophylline cocrystals. *CrystEngComm*, 16(22):4753-4765, 2014.

[27]   Yano, Y., Yoshida, M., Hoshino, S., Inoue, K., Kida, H., Yanagita, M., Takimoto, T., Hirata, H., Kijima, T., Kumagai, T., and Osaki, T. Anti-fibrotic effects of theophylline on lung fibroblasts. *Biochemical and Biophysical Research Communications*, 341(3):684-690, 2006.

[28]   Trask, A. V., Motherwell, W. D. S., and Jones, W. Physical stability enhancement

of theophylline via cocrystallization. *International Journal of Pharmaceutics*, 320(1-2):114-123, 2006.

[29] Das, B. and Baruah, J. B. Water bridged assembly and dimer formation in Co-crystals of caffeine or theophylline with polycarboxylic acids. *Crystal Growth and Design*, 11(1):278-286, 2011.

[30] Karki, S., Friščić, T., Jones, W., and Motherwell, W. D. S. Screening for pharmaceutical cocrystal hydrates via neat and liquid-assisted grinding. *Molecular Pharmaceutics*, 4(3):347-354, 2007.

[31] Delori, A., Frišić, T., and Jones, W. The role of mechanochemistry and supramolecular design in the development of pharmaceutical materials. *CrystEngComm*, 14(7):2350-2362, 2012.

[32] Bhogala, B. R. and Nangia, A. Cocrystals of 1,3,5-cyclohexanetricarboxylic acid with 4,4′ -bipyridine homologues: Acid···pyridine hydrogen bonding in neutral and ionic complexes. *Crystal Growth and Design*, 3(4):547-554, 2003.

[33] Childs, S. L., Stahly, G. P., and Park, A. The salt-cocrystal continuum: The influence of crystal structure on ionization state. *Molecular Pharmaceutics*, 4(3):323-338, 2007.

[34] Aakeröy, C. B., Fasulo, M. E., and Desper, J. Cocrystal or salt: Does it really matter? *Molecular Pharmaceutics*, 4(3):317-322, 2007.

[35] Stilinović, V. and Kaitner, B. Salts and Co-crystals of gentisic acid with pyridine derivatives: The effect of proton transfer on the crystal packing (and vice versa). *Crystal Growth and Design*, 12(11):5763-5772, 2012.

[36] Rietveld, H. M. A profile refinement method for nuclear and magnetic structures. *Journal of Applied Crystallography*, 2(2):65-71, 1969.

[37] *SAINT Plus, Bruker AXS Inc.: Madison, WI,* 2008.

[38] *BRUKER AXS (v 6.14); Bruker AXS Inc.: Madison, WI,* 2008.

[39]   *Barbour, L. J. X-Seed, Graphical Interface to SHELX-97 and POVRay; University of Missouri-Columbia: Columbia, MO,* 1999.

[40]   *Spek, A. L. PLATON, A Multipurpose Crystallographic Tool; Utrecht University: Utrecht, Netherland,* 2002.

[41]   Spek, A. L. and IUCr Single-crystal structure validation with the program *PLATON. Journal of Applied Crystallography*, 36(1):7-13, 2003.

Chapter 2 Part B

Pyridine *N*-Oxides as Coformer in the Development of Drug Cocrystals

2.B.1 Abstract

A convenient method is identified & applied in the synthesis of pyridine *N*-oxides. Among the synthesized pyridine *N*-oxides, 4,4'-bypyridine-*N*, *N*′-dioxide has been chosen as coformer to cocrystallize with several drug molecules such as propofol, ferulic acid, sulfathiazole, *p*-aminobenzoic acid etc. and presented in this study. These drugs are associated with aqueous solubility and bioavailability issues. Trends in aqueous solubility exhibited by them have been examined and correlated to different types of supramolecular heterosynthons present in these cocrystals. Hydrogen bond synthons such as COOH···pyridine *N*-oxide, OH or NH···pyridine *N*-oxide are found to be robust and followed the CSD trend. These synthons energies and contribution of weak interaction in cocrystals are correlated with the improved properties supported by DFT study and Hirshfeld surface analysis and presented.

2.B.2 Introduction

The heterocyclic *N*-oxides have substantial importance for their wide applicability as synthetic intermediate, protecting group, auxiliary agent, channel fluorosensor, oxidant, ligand in metal complex, catalyst etc. [1–5]. Besides that, they are found to have potential for various biological applications [6–9]. The finding of phenazine-*N*, *N*′-dioxides, as pro-drug for anti-tumour therapy and aspergillic acid, an antibiotic which is the tautomer of pyrazine-*N*-oxide, draws significant interest in the pharmaceutical aspects of heterocyclic *N*-oxides [9]. The synthesis *N*-oxides has been known for decades but an improved and convenient method is always a desire for a chemist. A plethora of studies on the synthesis of *N*-oxides using various oxidizing agents in varying reaction conditions has been reported. The most common oxidizing agents are peracetic acids, H_2O_2 and *m*-chloroperbenzoic acid (*m*-CPBA) etc. [10].

On the other hand, only a few reports are available which explored the *N*-oxides as potential coformers with the intention to synthesize pharmaceutical cocrystals driven by the formation of supramolecular heterosynthons [11–14]. Despite being strong hydrogen

bond acceptor, the application of *N*-oxides in the supramolecular synthesis in establishing interaction with functionalities viz. –OH, –COOH, –NH, –CONH$_2$ etc., has not been explored considerably. Thus, prospect to endure the development of *N*-oxide synthesis is ample. The *N*-oxides can be explored as potential coformers for cocrystal preparation driven by the formation of predicted supramolecular heterosynthons. Taking this into consideration, bottom-up synthesis of suitable coformers in the laboratory has emerged as one of the most productive approaches to engineer pharmaceutical cocrystals. In this part of Chapter 2, the synthesis of several pyridine *N*-oxides is reported. One of them, i.e. 4, 4′ bypyridine *N, N*-dioxide [BPNO] is employed as coformer to prepare cocrystals of drugs such as ferulic acid [FERU], sulfathiazole [SULF], *p*-aminobenzoic acid [*p*-ABA] and liquid drug propofol [PROP] having different functionality [15]. It is intended to examine how drug properties such as aqueous solubility vary with the formation of various supramolecular synthons. The present study is focused on the following two prime objectives: (i) usage of pyridine *N*-oxides as coformer for the synthesis of drug cocrystals, and (ii) exploit the formation of different hydrogen bond synthons between *N*-oxide and drug to amend physiochemical properties of the parent drug. We further report a convenient method of synthesis of pyridine *N*-oxides using *m*-CPBA as the oxidant in 1, 4-dioxane solvent.

2.B.3   Results and Discussion

2.B.3.1 Synthesis of Pyridine-N-oxides

Although many processes to synthesize *N*-oxides are already been reported in the literature using H$_2$O$_2$, peracetic acid and m-CPBA as oxidants, it is yet challenging to overcome associated limitations such as longer reaction time, use of catalysts, poor yield and tedious isolation technique.
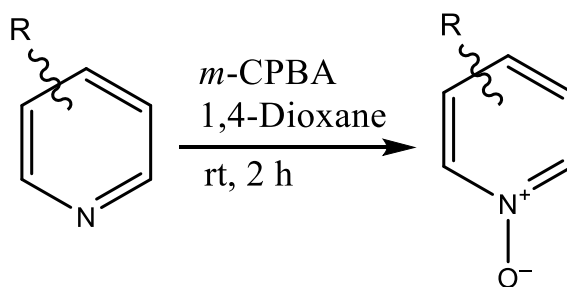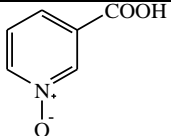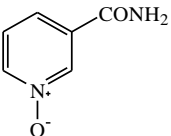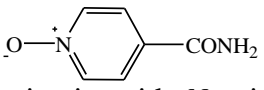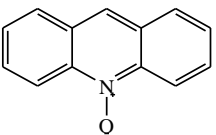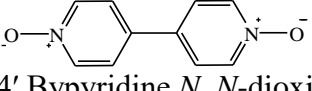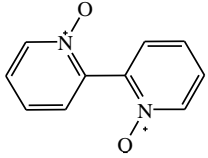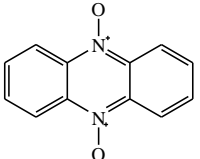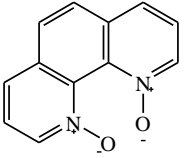
Scheme 2.B.1 Synthesis of pyridine *N*-oxides

Herein, a simpler method for the synthesis of *N*-oxides using meta chloro perbenzoic acid (*m*-CPBA) as oxidant and 1, 4-dioxane as the solvent is reported. This technique is found to be robust, simpler, time saving and efficient for the preparation of various *N*-oxides. Absolute amount of the substrate was added to about 5-7 mL of 1,4-dioxane and stir for few minutes at ambient condition. To this solution, a stoichiometric amount of *m*-CPBA was added and the homogeneous mixture was left stirring for about 30 minutes monitored by TLC for complete conversion of the substrates to its corresponding *N*-oxides (Scheme 2B.1). The precipitate obtained was filtered, washed with dioxane and dried for further characterization. Synthesized *N*-oxides are shown below in Table 2.B.1. Use of *m*-CPBA is compared with other oxidants such as potassium persulphate and hydrogen peroxide under same reaction conditions and found to be superior and a comparison is depicted in Appendix (Figure A.2). The solvent 1,4-dioxane is found to effective in terms of reaction completion time, milder condition and easy isolation of products. The solubility advantage of *m*-CPBA in 1,4-dioxane eases the separation process. The products are insoluble in 1,4-dioxane, whereas their starting materials and *m*-chlorobenzoic acid (*m*-CBA) are soluble. Therefore solubility differences in 1,4-dioxane make the separation more convenient.

2.B.3.2 Characterization of *N*-oxides

Synthesized *N*-oxides are characterized by using spectroscopy, thermal and X-ray diffraction tools. Typically the IR absorption of C=N and C−N moieties of pyridine-like ring is observed at approximately 1560 cm^{-1} and 1230 cm^{-1} and are consistent for all *N*-oxide products. The absorption band of N−O$_{stretching}$ in the region 1320-1225 cm^{-1} is the characteristic absorption of the aromatic *N*-oxides. Hence, the IR absorptions nearly at 1233, 1242, 1304, 1263, 1250, 1272, 1261 and 1263 cm^{-1} showed the formation of product entries **1**-**8** respectively. In ^{1}H-NMR spectroscopy, the deshielding of the aromatic proton (s) attached to the ortho position of N^{+}−O$^{−}$ moiety further confirms the formation of pyridine *N*-oxides (details are in experimental section 2.B.5.2). The elemental analyses for all the synthesized *N*-oxides are found to be satisfactory (details are in experimental section 2.B.5.2).

Table 2.B.1 Synthesis of pyridine *N*-oxides

Entry	Products	Yield (%)	Reaction Time (min)
1	Nicotinic acid *N*-oxide	65	20
2	Nicotinamide *N*-oxide	70	20
3	Isonicotinamide *N*-oxide	72	20
4	Acridine *N*-oxide	25	20
5	4, 4′ Bypyridine *N, N*-dioxide	92	20
6	2, 2′ Bypyridine *N, N*-dioxide	70	20
7	Phenazine *N, N*-dioxide	85	20
8	1, 10 Phenanthroline *N, N*-dioxide	32	120

In addition to spectral analysis, the synthesized *N*-oxides have been confirmed by single crystal X-ray diffraction. Single crystals of **1**, **2**, **3**, **4**, **5**, **6**, and **8** suitable for X-ray diffraction are grown from suitable solvents and their crystal unit cell parameters are determined. The Cambridge Crystallographic Database analysis shows single crystal

structures for the product *N*-oxides, entry **4** and **7** were not reported. We deferred to recollect single crystal data for reported molecules **1** (CSD refcode VATNUA) [16], **2** (CSD refcode MEGDEI), **3** (MEGDAE) [12], **5** (BAFVUZ) [17] and **8** (LAQHUG) [18]. The suitable crystals for entry **7** could not be grown but the structure for entry **4** was evaluated (Figure 2.B.1). The *N*-oxide molecules are generally hygroscopic in nature because of the only availability of strong hydrogen bond acceptor group (N^+-O^-) and for comparison, we have determined the structure of entry **6** again [VAGQAW, see the crystal structure analysis section, Figure 2.B.2]. The single crystals of acridine *N*-oxide dihydrate (Entry **4**) have been isolated from slow evaporation of methanol. The structure is primarily guided by strong $\pi\cdots\pi$ and O−H⋯O hydrogen bonds (Figure 2.B.2). Acridine molecules are stacked along [010] crystallographic axis. The N^+-O^- moiety from an alternate molecule is oriented in one direction and connected by continuous water chain via strong O−H⋯O hydrogen bonds.

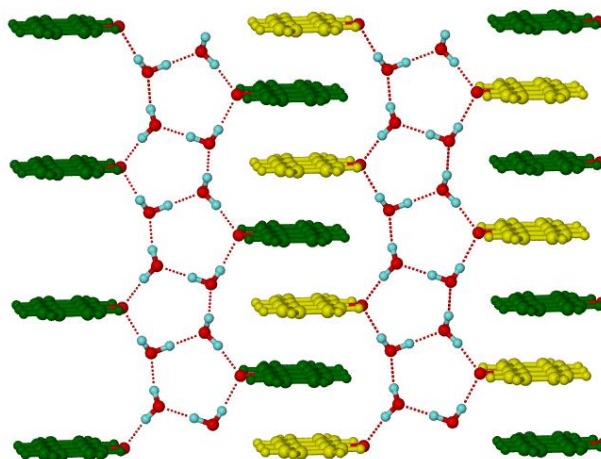**Figure 2.B.1** The $\pi\cdots\pi$ stacking and O−H⋯O hydrogen bonds dominate the crystal structure of acridine *N*-oxide dihydrate.

A similar trend of water chain involvement in connecting host molecules to complete the molecular packing is also observed in 2,2'-bipyridine-*N*, *N*'-dioxide crystal structure (entry 6, Figure 2.B.2). The electronegative oxygen of *N*-oxide acts as a dual acceptor in the former structure, whereas it is single in later structure. Information of crystallographic parameters for all structures is furnished in Appendix Table A.2
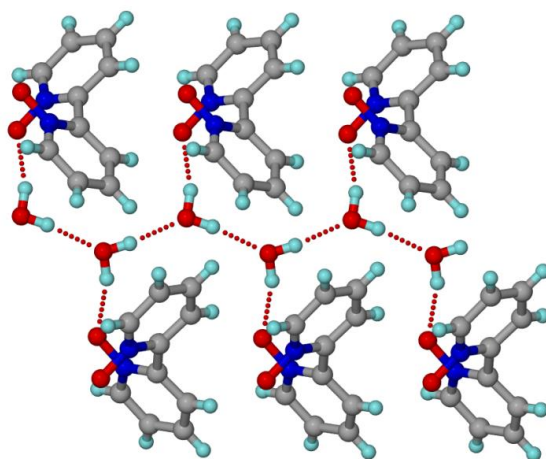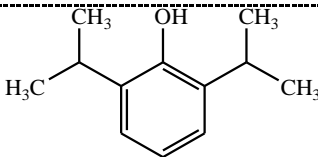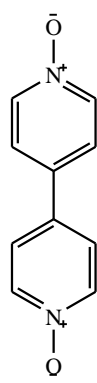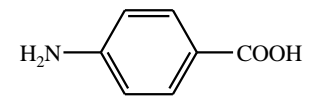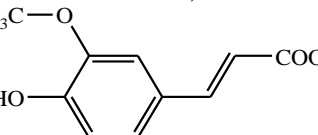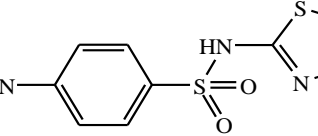
Figure 2.B.2 Water chain connects host molecules via O−H···O hydrogen bonds in the crystal structure of 2,2'-bipyridine-*N, N'*-oxide monohydrate.

2.B.4   Synthesis of *N*-oxide Cocrystals

Cocrystals are generally formed via the formation of hydrogen bonds between drug and coformer to alter the physiochemical properties, while the structural features of the parent molecules remain. The N^+-O^- moiety of pyridine *N*-oxide possesses a unique and strong pull property that has an essential chemical consequence with hydrogen bond donor groups in the subject of cocrystal technology. The *N*-oxide often provides better drug-like behaviour by enhancing physiochemical and pharmacokinetic properties. The strong receptor affinity by N^+-O^- moiety at the binding site causes good intermolecular interactions with the drug molecule could be the reason for better drug-like behaviour. Besides their medicinal values, the receptor affinity by N^+-O^- moiety of *N*-oxide has recently exploited to make predictable cocrystals with carboxamides and sulphonamides [12,13]. The scope of the carboxamide···pyridine-*N*-oxide supramolecular heterosynthon in amide-containing drug molecules and sulfonamide with pyridine-*N*-oxide as cocrystal former was also examined [11]. The bipyridine-4,4'-*N, N'*-dioxide [BPNO] shows significant flexibility as a supramolecular connector because they easily form strong hydrogen bonds with C−H, N−H, O−H, S−H etc. donors. Besides strong hydrogen bond formation with acceptor N^+-O^-, they show the possibility to stack molecules by aromatic $\pi\cdots\pi$ interaction. Therefore, the BPNO is chosen to exploit as coformer for different drugs.

Four drugs are chosen to prepare cocrystals with *N*-oxides considering the availability of different functional groups and their associated shortcomings in physiochemical properties like poor aqueous solubility, bioavailability etc.

Table 2.B.2 Four stoichiometry cocrystals of drugs propofol, *p*-aminobenzoic acid, ferulic acid and sulfathiazole were isolated with BPNO [**C1**, **C2**, **C3** and **C4** respectively].

Drug	Coformer	Cocrystal/ stoichiometry
Propofol (PROP)	4, 4′ bypyridine *N, N′*-dioxide (BPNO)	C1 [4:1 PROP:BPNO]
p-Aminobenzoic acid (*p*-ABA)		C2 [2:1 *p*-ABA:BPNO]
Ferulic acid (FERU)		C3 [1:1 FERU:BPNO]
Sulfathiazole (SULF)		C4 [1:1 SULF:BPNO]

Propofol (PROP) is a liquid drug and readily used as an intravenous anaesthetic, marketed as Diprivan [19]. Generally, it is administered through injection. However, due to its poor aqueous solubility, it causes discomfort on injection and it is a major demerit of it [19]. In addition to it, the emulsion formulation of the drug requires efforts to arrange container system such as multi-layer plastic containers with lower waste disposal costs etc. As solid crystalline forms are always preferred than a liquid/solution, we herein demonstrated synthesis of cocrystals of propofol (Table 2.B.2), with *N*-oxide relies on the fact that the phenolic ─OH can undergo strong intermolecular interactions *via* O─H···pyridine *N*-oxide hydrogen bond. This would certainly ease the incompatibilities of liquid drugs without axing the originality of the drug. Cocrystal **C1** reported here as a proof of this insight. Only the cocrystal of isonicotinamide with propofol has been

reported with the emphasis of liquid drugs into solid formulations prior to this study [20]. Apart from propofol, three other drug ferulic acid (FERU), sulfathiazole (SULF) and *p*-aminobenzoic acid (PABA) were considered for cocrystal synthesis. Because of the presence of phenolic OH, COOH, NH_2 and sulfonamide groups in these drug molecules, cocrystals formation is predictable by the formation of different supramolecular synthons.

2.B.4.1 Characterization of *N*-Oxide Cocrystals

Cocrystals of drugs propofol [PROP], *p*-aminobenzoic acid [PABA], ferulic acid [FERU] and sulfathiazole [SULF] in 4:1, 1:1, 1:1 and 1:1 respectively were isolated with BPNO [**C1**, **C2**, **C3** and **C4** respectively]. They are characterized by spectroscopy, thermal analysis and X-ray diffraction and then subjected for aqueous solubility determination. The single crystal structure of **C2** has been reported by Manuel et al. in the year 2003 [21]. This material **C2** has been re-synthesize in pure phase and characterized for a consistent comparison of property exhibited by them. The drug *p*-ABA comprises with NH and COOH groups, which simultaneously interact with *N*-oxides.
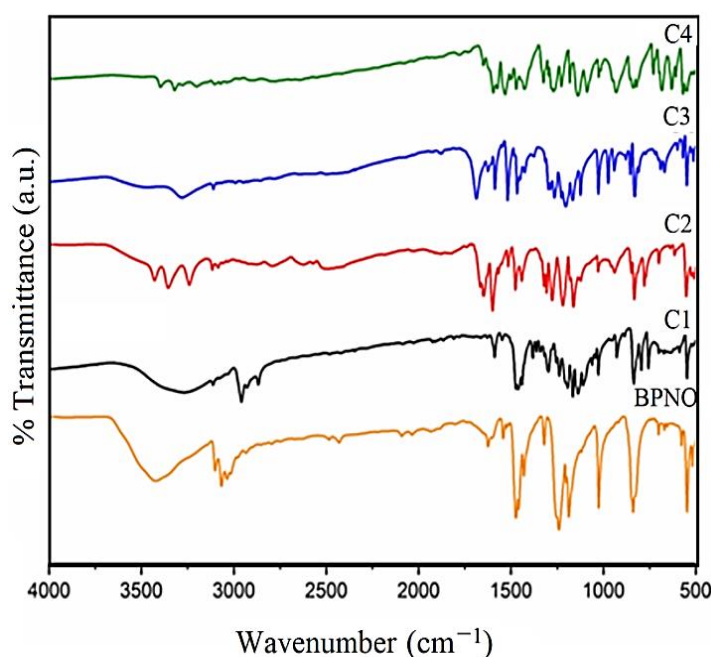

Figure 2.B.3 FT-IR spectra of cocrystal materials **C1**, **C2**, **C3** and **C4** compared with BPNO

The significant shifting of major stretching vibrations in the FT-IR spectroscopy for interacting functional groups in the cocrystals indicated their formation (Figure 2.B.3). The O−H stretching vibrations and C−O−H bending vibration modes for pure PROP molecule appear at 3574 and 1441 cm^{-1}. Lowering of O−H stretching frequencies in cocrystals attributed the formation of intermolecular OH···pyridine *N*-oxide hydrogen bond synthon. In cocrystal **C2** and **C3**, –C=O stretching frequency appears at 1660 and 1687 cm^{-1} indicating the participation of –COOH group in intermolecular hydrogen bonding. The asymmetric and symmetric N−H stretching vibrations of **C4** are observed in the range 3397 cm^{-1} and 3322 cm^{-1} respectively, due to intermolecular hydrogen bonding. Details of all major stretching vibrations are described in experimental section 2.B.5.5.

The differential scanning calorimetry (DSC) plots show single endothermic melting peaks for the cocrystals (Figure 2.B.4). Trace methanol solvent adsorbed on the crystal surface of C3 was detected as a small endotherm at ~50 °C. The features after the melting endotherms of cocrystals C1 and C2 are due to thermal decomposition. All the cocrystal materials show totally different melting behaviour from their starting compounds, which endorse the formation of pure cocrystal phases. A melting point comparison of cocrystal and starting materials is incorporated in Table 2.B.3
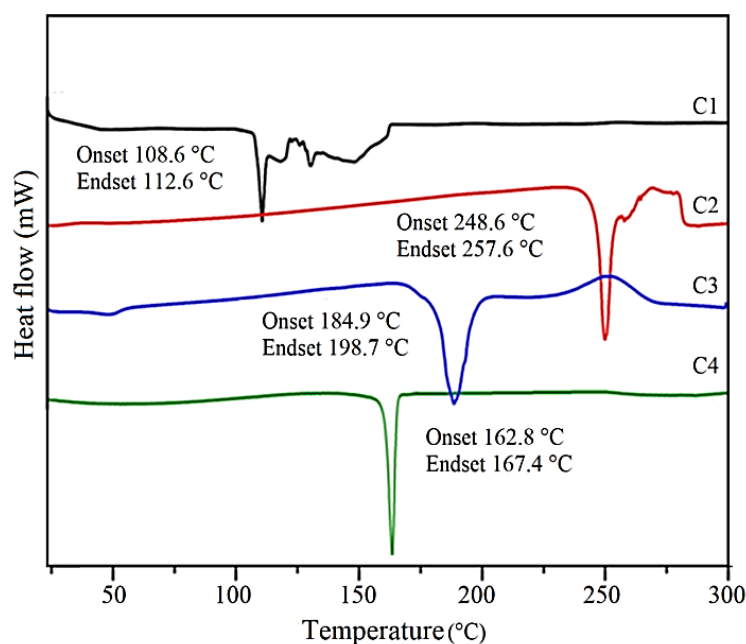

Figure 2.B.4 DSC endotherms represent melting onset of *N*-oxide cocrystals.

Table 2.B.3 Comparison of drug and melting onset of the cocrystals

Coformer	Drug	Melting point °C	Cocrystal	Melting point °C	
				Onset	**Endset**
	PROP	17–18	**C1**	108.6	112.6
BPNO [298–306 °C]	PABA	187–189	**C2**	248.6	257.6
	FERU	168–172	**C3**	184.9	198.7
	SULF	200–202	**C4**	162.8	167.4

The grinded cocrystal materials are analysed by PXRD and compared with the starting materials. Different PXRD patterns are observed for the materials compared to the starting materials indicating the formation of pure cocrystal phases. The experimental PXRD patterns of cocrystal materials are further compared with those simulated from the single-crystal structures. The overlaid patterns generated from single crystal structure and experimental PXRD patterns showed the same peak position and intensity profile. A good agreement with the simulated pattern indicated the purity of the phase and shown in Appendix (Figure A.3).
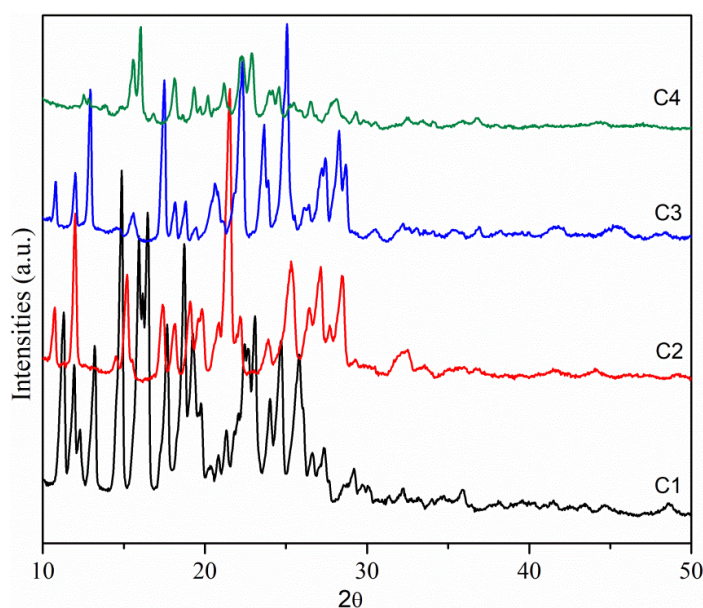
Figure 2.B.5 PXRD patterns of **C1**, **C2**, **C3** and **C4**.

The formation of the COOH−pyridine-*N*-oxide, phenol OH···pyridine-*N*-oxide and amine NH···pyridine-*N*-oxide single point heterosynthon seems to be obvious if there is no other hydrogen bond competition. *N*-oxide bears mostly single or dual hydrogen bond acceptor ability. Hydrogen bond synthons constructed by these functional groups (i.e. −COOH, −NH₂, −OH groups) with *N*-oxide in organic cocrystal systems are picked from

CSD and their occurrence probability is determined and summarized in Figure 2.B.10. The probabilities are compared with already reported synthons produced by $-CONH-$, $-SO_2NH-$ groups with *N*-oxides [11–13]. Nearly 14% probability of phenol OH$-$pyridine-*N*-oxide synthon (synthon VII, *N*-oxide as a dual acceptor) in organic cocrystals is observed from this study. The value rises to 37% when there is no other functional group present. If $-OH$ group is replaced by $–COOH$ the occurrence probability increases to 24% (synthon IV) in presence of other functional groups. It can go up to 64% if no competing functional group is present in the system, signifying the dominance of COOH⋯pyridine-*N*-oxide synthon. The occurrence probability of phenol OH⋯pyridine *N*-oxide synthon, where *N*-oxide acts as a dual acceptor are found to be approximately double than the single acceptor if no competing functional groups are available on the substrate. But the NH_2⋯pyridine-*N*-oxide synthon where *N*-oxide acts as two and three hydrogen bond acceptor is not perceived for aromatic amines (synthon VII). However, in case of most of the aliphatic amines, this observation is not consistent.

Drug propofol has the OH donor and thereby OH$-$pyridine-*N*-oxide heterosynthon II dominates in **C1** (Figure 2.B.6). In presence of phenolic OH or $–NH_2$ the occurrence probability of heterosynthon IV raised by 2 fold (53%), as OH stabilizes it by constructing a two-point synthon i.e. VIII. The COOH⋯pyridine-*N*-oxide and sulfonamide or carboxamide NH$-$pyridine⋯*N*-oxide heterosynthons are the strongest interactions. These interactions are observed in **C2** and **C3** cocrystals that can be exploited to construct designed cocrystals of pharmaceutical relevance because they are reliable. This is because of the best hydrogen bond donor ability of carboxylic OH and sulfonamide NH and acceptor ability of the *N*-oxide. In presence of best donor groups such as COOH, the *N*-oxide is expected to behave as single hydrogen bond acceptor. But nearly 55% occurrence probability of the two-point N$-$H⋯O heterosynthon [graph set $R_2^2(8)$] supported by auxiliary C$-$H⋯O is observed in COOH⋯pyridine-*N*-oxide systems (synthon I). Surprisingly the synthon with [$R_2^2(8)$] graph set notation is not found in any of the reported sulfonamide⋯pyridine *N*-oxide or carboxamide⋯pyridine *N*-oxide systems (Synthon II & III). The nonplanarity of the sulfonamide group and availability of NH donor perhaps prevent the formation of two-point hydrogen-bonded cyclic motif with *N*-oxide. Presence of OH and NH groups changes the role of *N*-oxide

to dual acceptor (synthon VIII). Though COOH group is planner, the $[R_2^2(8)]$ synthon is absent in any of the **C2** and **C3** structures (Figure 2.B.7 & 2.B.8). This is because to satisfy hydrogen bond donor⋯acceptor rules, instead of going for two-point N−H⋯O + C−H⋯O cyclic heterosynthon, the C=O of carboxylic acid accepts either NH or OH donors respectively.

To support these synthon recurrence probabilities we performed DFT calculation for the synthon energies. The synthon energies are in good agreement with the high recurrence probability of synthon I ($E_{COOH\ldots N\text{-}oxide}$ dimer = −11.29 Kcalmol^{-1}), IV ($E_{COOH\ldots N\text{-}oxide}$ = −8.91 Kcalmol^{-1}), V ($E_{CONH\ldots N\text{-}oxide}$ = −6.40 Kcalmol^{-1}), VI ($E_{SO2NH\ldots N\text{-}oxide}$ = −11.36 Kcalmol^{-1}), VIII ($E_{COOH\ldots N\text{-}oxide}$ + $E_{NH\ldots N\text{-}oxide}$ = −12.11 Kcalmol^{-1}). Whereas the synthon constructed by single point connection between N-oxide to phenolic OH or aniline NH seems to establish a strong interaction ($E_{phenolic\ OH\ldots N\text{-}oxide}$ = −6.46 Kcalmol^{-1}; $E_{aniline\ NH\ldots N\text{-}oxide}$ = −5.14 Kcalmol^{-1}).
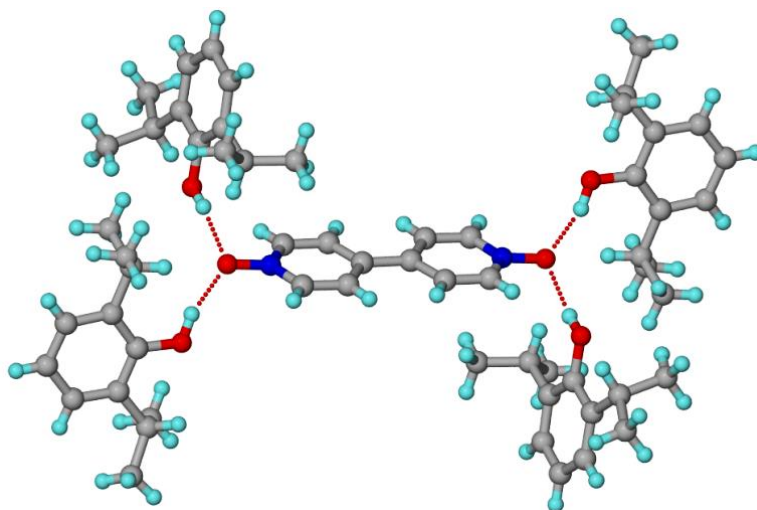

Figure 2.B.6 The *N*-oxide acts as a dual hydrogen bond acceptor as the OH groups from two propofol molecules are connected to *N*-dioxide via a dominating O−H⋯O interaction in **C1**.
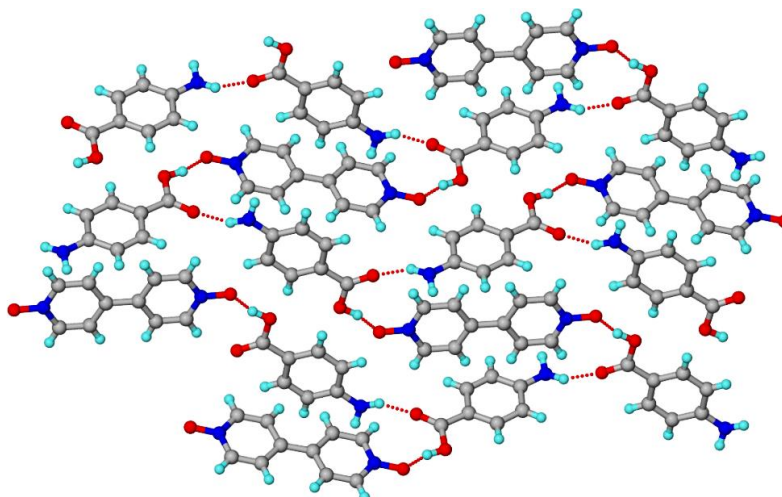
Figure 2.B.7 Carboxylic acid−*N*-dioxide single point hydrogen bond prevails in cocrystal **C2**. The C=O accepts the N–H via N−H···O hydrogen bond.
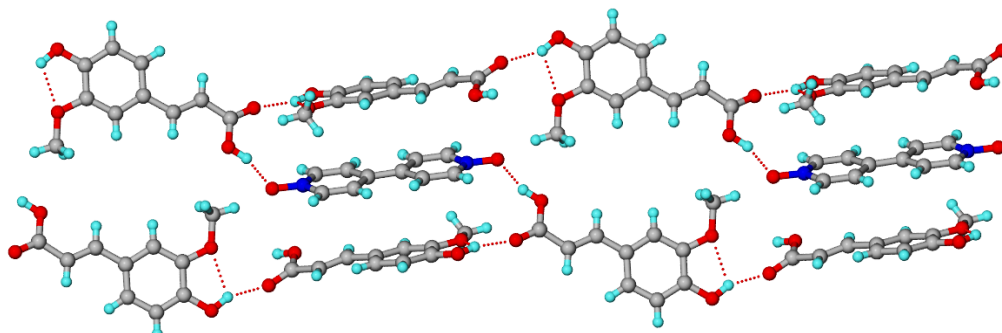

Figure 2.B.8 Similar to **C2**, the C=O group of COOH accepts the OH via O−H···O hydrogen bond. Whereas single point interaction between COOH and *N*-oxide retains in cocrystal **C3**.

Generally, the imide tautomer is observed as robust in all sulfathiazole polymorphs [22]. In **C4**, the proton of sulfonamide group resides on the five-membered ring nitrogen and molecules are connected via N−H···N and N−H···O=S hydrogen bonds (Figure 2.B.9). But, on introducing strong hydrogen bond acceptor group *N*-oxide, the N−H···O$_{\text{N-oxide}}$ hydrogen bond synthon formed. The reasons for the formation of this synthon can be attributed due to the interactions that exist between the strongest donor (NH, the proton from ring nitrogen; E = −11.36 Kcalmol^{-1}) and the strongest acceptor (O$^-$ of *N*-oxide). From the analysis, it is evident that under a certain condition or varying functionalities, it is possible to manipulate the molecules to recognize and bind by tuning the strength of site-specific complementary hydrogen bond functionality or the competing intermolecular interactions.
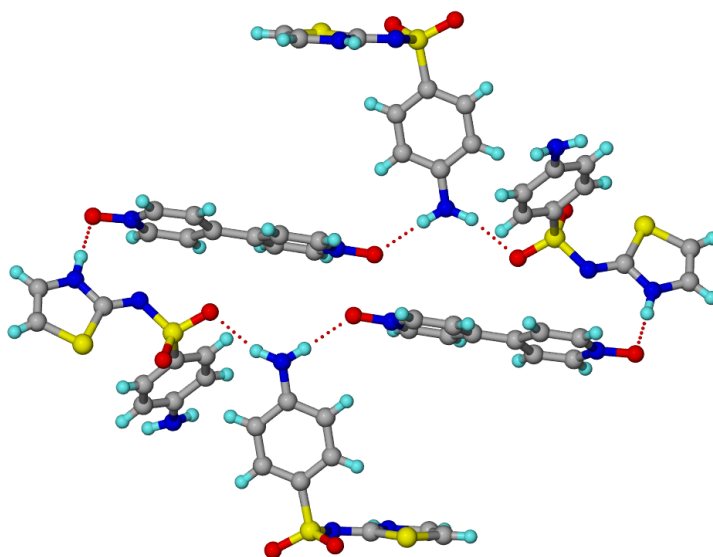
Figure 2.B.9 The 5 member ring NH proton of sulfathiazole bears strongest donation ability; thereby in **C4** the formation of $NH_{imide} \cdots N$-oxide synthon dominates. However, $NH_{amine} \cdots N$-oxide synthon competes with $NH_{imide} \cdots N$-oxide.

Though the carboxylic acid−pyridine *N*-oxide cyclic heterosynthon motif (synthon I) is not observed in **C2**, and **C3** cocrystals, the bimolecular recognition is expected between molecules containing these two functional groups via $O-H_{COOH} \cdots O_{Noxide}$ (Figure 2.B.10). The $N-H_{imide} \cdots O_{Noxide}$ in **C4** is also formed in a predictable manner for designing cocrystals (Figure 2.B.9). Another set of experiment was carried out to investigate the existence of polymorphism in cocrystal materials as *p*-aminobenzoic acid and sulfathiazole are polymorphic coformer. As a preliminary observation, their cocrystals show no polymorphism based on the number of cocrystallization experiments. The reason is that the recurring COOH⋯pyridine *N*-oxide, OH⋯pyridine *N*-oxide or NH⋯pyridine *N*-oxide synthons in the structures are quite strong and predictable; which restricts their formation in a certain fashion only.

Table 2.B. 4 Hydrogen bond matrices of entries **4**, **6** and cocrystals **C1**-**C4**

N-Oxide/ Cocrystal	Interaction	H···A/Å	D···A/Å	∠D–H···A/°	Symmetry code
Entry **4**	$O_3–H_{1A}···O_1$	1.79	2.762(3)	170	1/2-x,1/2+y,1/2-z
	$O_3–H_{1B}···O_2$	1.88	2.854(3)	168	-
	$O_2–H_{2A}···O_1$	1.82	2.801(3)	174	1/2-x,-1/2+y,1/2-z
	$O_2–H_{2B}···O_3$	1.81	2.795(3)	179	1/2-x,-1/2+y,1/2-z
Entry 6	$O_2–H_{2A}···O_2$	1.88	2.855(1)	171	1/2-x,-1/2+y,z
	$O_2–H_{2B}···O_1$	1.82	2.778(1)	163	-x,y,1/2-z
	$C_2–H_2···O_1$	2.30	3.302(1)	154	-x,-1+y,1/2-z
	$C_5–H_5···O_1$	2.14	3.216(2)	170	-x,1-y,1-z
C1	$O_1–H_{1A}···O_3$	1.83	2.676(10)	158	–
	$O_2–H_{2A}···O_3$	1.90	2.731(1)	154	1-x,-1/2+y,1/2-z
	$O_2–H_{2A}···N_1$	2.62	3.334(1)	138	1-x,-1/2+y,1/2-z
	$C_7–H_7···O_3$	2.39	3.296(1)	153	–
	$C_{19}–H_{19}···O_3$	2.39	3.337(1)	162	1-x,-1/2+y,1/2-z
	$C_{29}–H_{29}···O_2$	2.58	3.184(1)	123	1-x,1/2+y,1/2-z
C2	$N_2–H_{1A}···O_3$	2.09	2.958(10)	156	x,1/2-y,1/2+z
	$N_2–H_{2A}···O_1$	2.26	3.055(2)	152	1-x,-1/2+y,1/2-z
	$O_4–H_{3A}···O_1$	1.73	2.590(3)	155	1/2-x,1-y,-1/2+z
	$C_1–H_1···O_3$	2.59	3.420(11)	149	1/2+x,1/2-y,-z
	$C_5–H_5···O_3$	2.41	3.279(11)	157	1/2-x,1-y,1/2+z
C3	$O_4–H_{3A}···O_6$	1.83	2.677(2)	155	-1+x,1/2-y,-1/2+z
	$O_7–H_{4A}···O_5$	1.73	2.588(2)	157	1-x,-1/2+y,3/2-z
	$C_{10}–H_{10}···O_7$	2.53	3.244(2)	134	x,1/2-y,-1/2+z
C4	$N_1–H_{1A}···O_4$	2.03	2.909(4)	170	1-x,1-y,-z
	$N_1–H_{2A}···O_6$	2.09	3.030(4)	163	-1/2-x,-1/2+y,1/2-z
	$N_3–H_{3A}···O_3$	1.79	2.722(3)	175	1/2-x,-1/2+y,1/2-z
	$N_3–H_{3A}···N_4$	2.43	3.246(3)	145	1/2-x,-1/2+y,1/2-z
	$C_{10}–H_{10}···O_1$	2.45	3.293(3)	150	1/2-x,-1/2+y,1/2-z
	$C_{14}–H_{14}···O_4$	2.43	3.346(4)	167	-1+x,y,z
	$C_{17}–H_{17}···O_3$	2.51	3.390(4)	159	1+x,y,z

Synthon I
(E = -11.29 Kcalmol^{-1})
(55%)

Synthon II
(0%)

Synthon III
(0%)

Synthon IV
(E = -8.91 Kcalmol^{-1})
(24%)

Synthon V
(E = -6.40 Kcalmol^{-1})
(67%)

Synthon VI
(E = -11.36 Kcalmol^{-1})
(40%)

Synthon VII
(X = O; 14%; E = -6.46 Kcalmol^{-1}; if N-oxide O$^-$
accepts only one OH)
(X = N; 0%; E = -5.14 Kcalmol^{-1}; if N-oxide O
$^-$accepts only one NH)

Synthon VIII
(X = O; 17%)
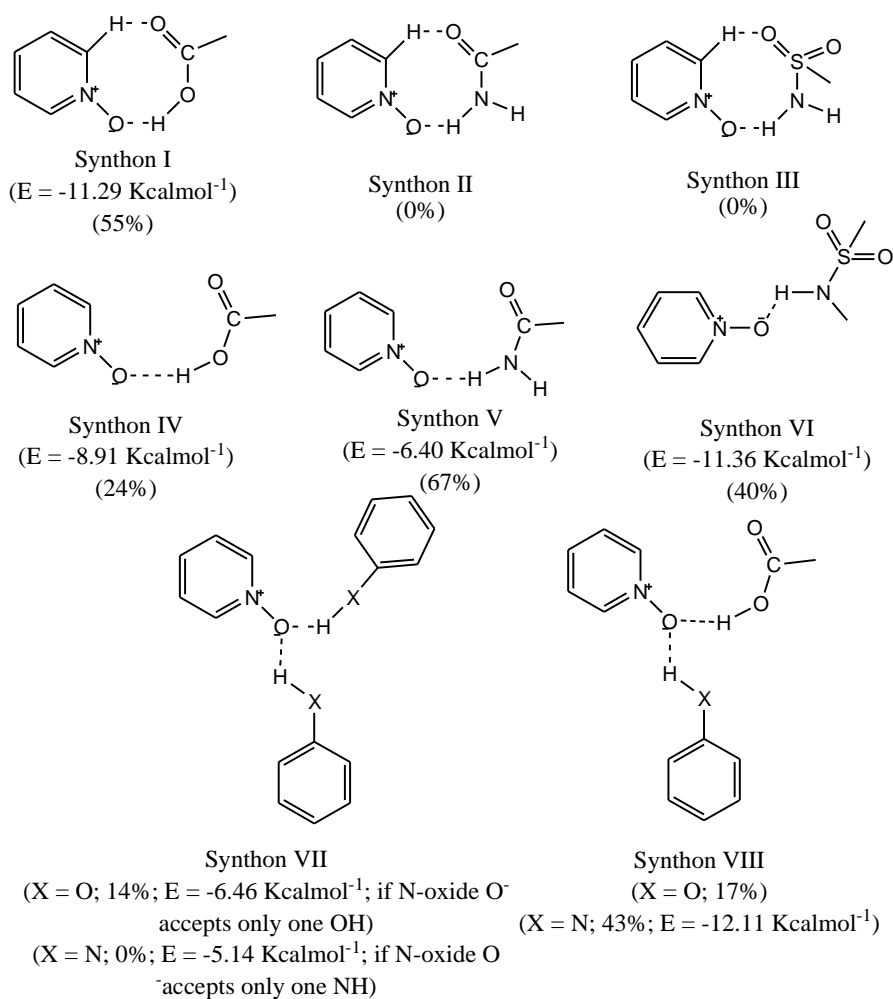(X = N; 43%; E = -12.11 Kcalmol^{-1})

Figure 2.B.10 Hydrogen bond synthons formed between heterocyclic *N*-oxide with –COOH, –CONH–, –SO$_2$NH–, and phenolic –OH or–NH containing coformers in organic cocrystals. The occurrence probability of the synthons is calculated from the crystal structure database that includes the structures presented in this study. Values along with hydrogen bond energies are given in bracket.

2.B.4.2 Hirshfeld Analysis

Analysis of molecular crystal structures using Hirshfeld surfaces is gaining popularity due to its usefulness in calculating the internuclear distances, angles, and identification of intermolecular interactions, which are considered to be very important in structure-activity research [23]. The molecular crystal structures of cocrystals **C1**-**C4** are considered for quantitative analysis of intermolecular interactions using Hirshfeld surfaces. The 2D fingerprint plots, which are derived from the Hirshfeld surfaces, are unique for each cocrystal and presented in Figure 2.B. 12.
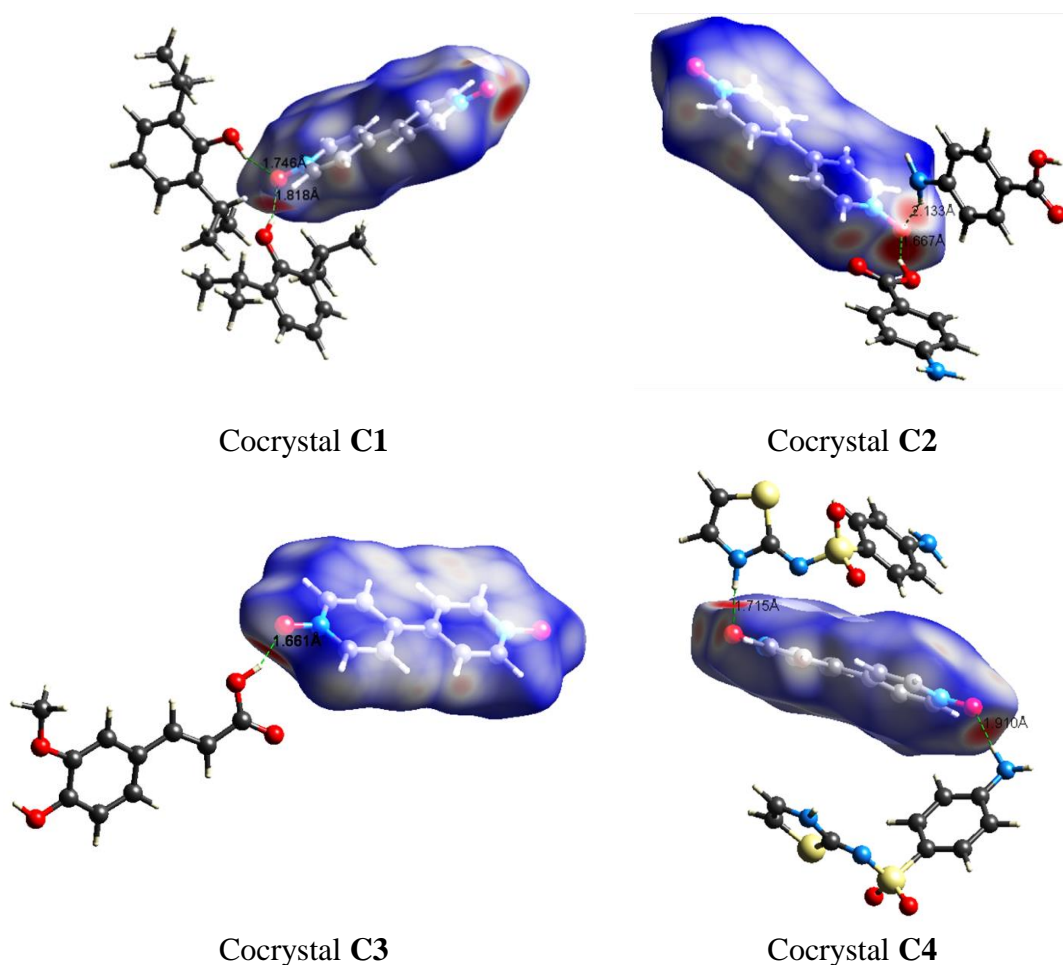
Cocrystal **C1**   Cocrystal **C2**

Cocrystal **C3**   Cocrystal **C4**

Figure 2.B.11 The COOH⋯pyridine *N*-oxide, OH⋯pyridine *N*-oxide or NH⋯pyridine *N*-oxide interactions present in cocrystals **C1**-**C4** are derived from Hirshfeld surfaces.

A lower degree of interactions with polar solvents is expected for **C1** and **C3** cocrystals because of the minuscule contribution of O⋯H interaction (6.6% and 13.5% respectively) in comparison with **C2** and **C4** (27.1% and 29.4% respectively). Being fascinated about the use of these interaction parameters in real consequences, particularly in physiochemical property prediction of cocrystals, we intended to determine the aqueous solubility for the cocrystals. It looks **C1** and **C3** might show lower aqueous solubility. However, the higher contribution of O⋯H interactions advocates better interaction possibility with polar solvents. Thus, it is anticipated that cocrystal **C2** and **C4** will have better aqueous solubility. The difference in polar and/or non-polar bonding contribution in cocrystal structure ensured a difference in drug⋯coformer or cocrystal⋯solvent interactions.

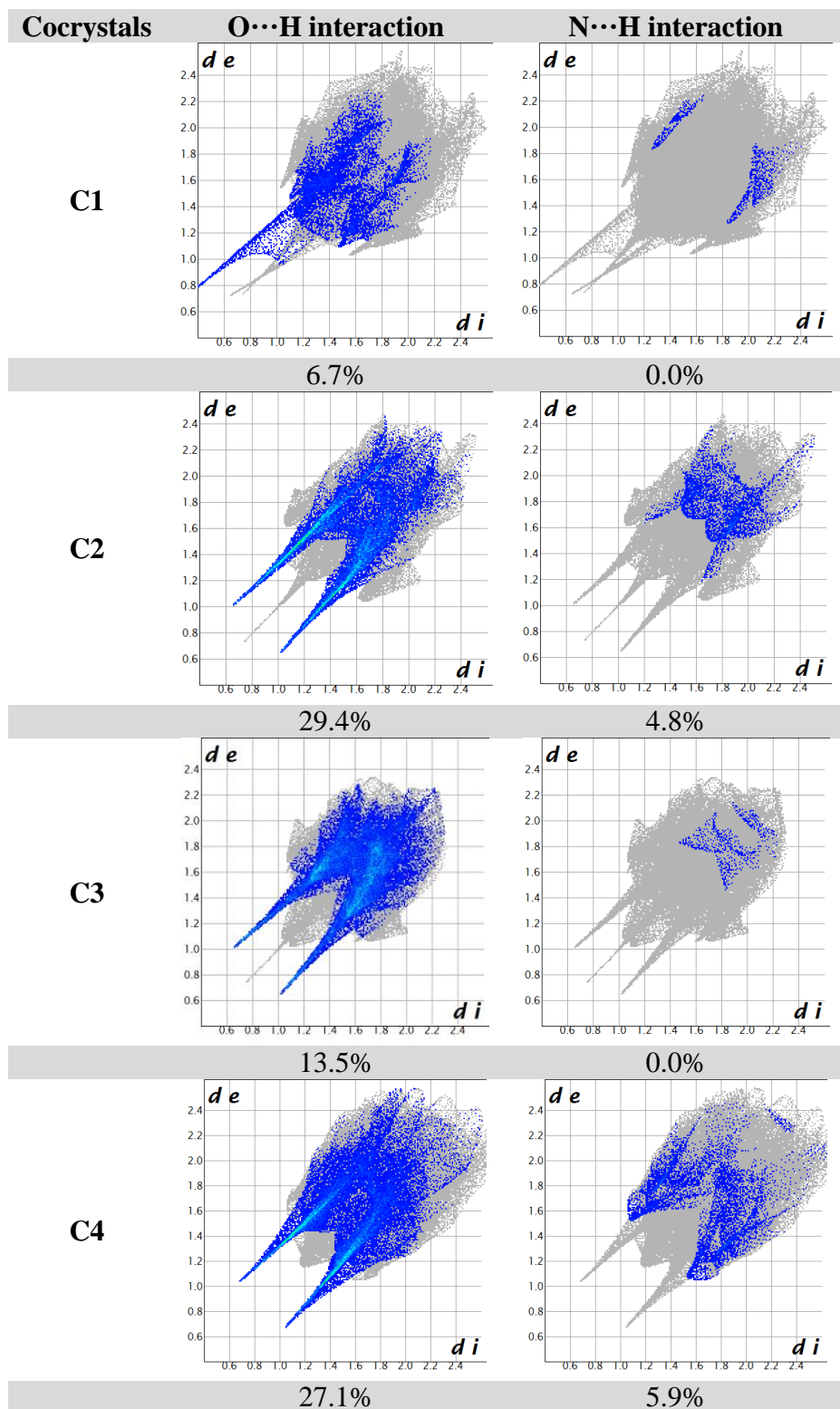**Figure 2.B.12** Hirshfeld surfaces show high O···H interaction contributions in **C2** and **C4** cocrystals leading to favourable interactions with polar solvents. This results in higher aqueous solubility of the cocrystals.

2.B.4.3 Aqueous Solubility

Standard aqueous solutions of concentration 0.05 mmol, 0.1 mmol, 0.2 mmol of cocrystals **C1**-**C4** are prepared to construct the absorbance vs. concentration calibration graphs using UV-Vis spectroscopy. Each experiment was performed in a jacketed, circulating flask maintained at 25 °C and in 3 sets to assure consistency. The 0.45 μm syringe filtered aliquot of cocrystal solution was taken for absorbance determination. The absorbance of the unknown solution was then correlated with the calibration curve obtained from the standard solution to evaluate the solubility concentration of cocrystal. Values determined from UV experiments were cross-checked by a series of gravimetric analysis for coherency. Interestingly, cocrystals **C1**-**C4** show improved solubility than the parent drug. The **C1** and **C4** show nearly 30 times higher solubility than propofol and sulfathiazole respectively. High contribution of polar interaction i.e. O···H and N···H could be the reason for the better interacting propensity of cocrystal towards water ensuing high solubility (Figure 2.B.13). Similarly, cocrystal with *p*-ABA and FERU showed high solubility.
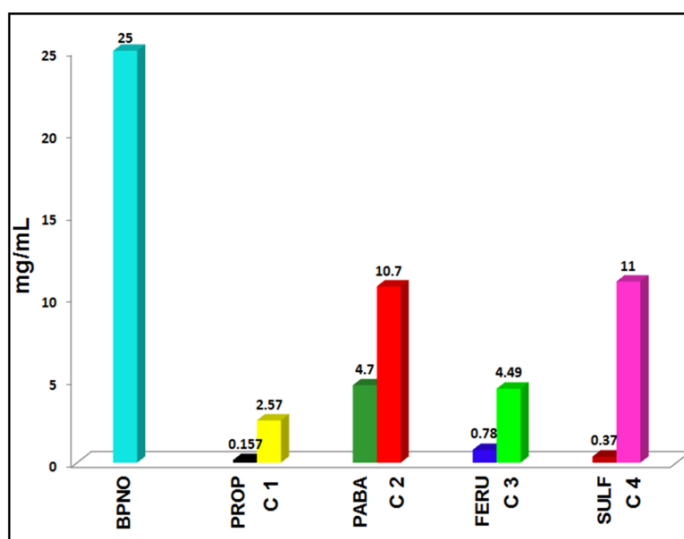

Figure 2.B.13 Aqueous solubility comparisons of drug and *N*-oxide cocrystals **C1**-**C4**.

2.B.5   Summary

A crystal engineering strategy is applied for the cocrystal synthesis of various drugs with coformer that are less explored, however pharmaceutically acceptable heterocyclic *N*-oxide functional group. For the synthesis of this coformer, i.e. heterocyclic *N*-oxide, a convenient methodology has been identified and implemented. The different types of

heterosynthons exhibited by the cocrystals of *N*-oxide-drug are analysed and compared with the structural database. The recurring COOH⋯pyridine *N*-oxide, OH or NH⋯pyridine *N*-oxide synthons in the structures are quite robust and predictable. Therefore, the reliability of formation of these supramolecular synthons pioneers for a new class of organic cocrystals that to be explored in the development of pharmaceutical industries. The modified biopharmaceutical property such as aqueous solubility of the drug is linked with the interaction contributions, which is a growing concern in the research & developments for academia and drug manufacturer. The cocrystal **C1** will provide further acquaintance with the amendment of liquid drugs into solid formulation *via* pharmaceutical cocrystallization approach. The scope of the present study can be easily extendable to dozens of *N*-oxide molecules as well as drugs, in particular, those which are associated with biopharmaceutical issues.

2.B.6 Experimental Section

2.B.6.1 Materials

The *N*-heterocyclic compounds and drug molecules used in this study were purchased from Sigma Aldrich, Himedia and Alfa-Aesar and used as received. The analytical-grade solvents were obtained from Merck. Millipore water was used for crystallization and solubility experiments.

2.B.6.2 N-oxide Cocrystal Synthesis

The BPNO was chosen as a representative coformer from the synthesized pyridine *N*-oxides listed in Table 2.B.1. Four cocrystals were isolated with drug propofol (**C1: PROP•BPNO**), *p*-aminobenzoic acid (**C2: PABA•BPNO**), ferulic acid (**C3: FERU•BPNO**), and sulfathiazole (**C4: SULF•BPNO**) respectively (Table 2.B.2). Starting materials were taken in stoichiometric ratios individually in a mortar and pestle. The mixture was grinded for 20-25 minutes and allowed for crystallization from methanol. We further examined the probability of occurrence of different stoichiometry cocrystals and/or cocrystal polymorph by changing the crystallization media and different starting materials ratios. Cocrystal **C1** afforded as 4:1 drug•coformer ratio, while the rest resulted only in 1:1 stoichiometry.

2.B.6.3 N-oxides Characterization

Synthesized N-oxides are characterised by employing various analytical techniques such as FT-IR, NMR spectroscopy, elemental analysis and single crystal x-ray diffraction. Elemental analysis was performed by using Perkin Elmer, USA Model: 2400 series 2. Following are the FT-IR, NMR spectroscopy, elemental experimental details.

Nicotinic acid-*N*-oxide: Yield % = 65; FT-IR (KBr, cm^{-1}): 464, 1273, 1484, 1576, 1716, 3079.

^{1}H-NMR (400 MHz, DMSO-d_6): δ (ppm) =7.50 (t, 1H, *J* = 6.8 Hz), 7.72 (d, 1H, *J* = 8.8 Hz), 8.38 (d, 1H, *J* = 7.2 Hz), 8.43 (s, 1H).

^{13}C-NMR (100 MHz, DMSO-d_6): δ (ppm) = 126.1, 127.2, 131.1, 139.4, 142.6, 165.0.

Elemental analysis: C, 51.80; H, 3.62; N, 10.07; O, 34.50.

Nicotinamide-*N*-oxide: Yield % = 70; FT-IR (KBr, cm^{-1}): 498, 814, 884, 930, 1686, 3136.

^{1}H-NMR (400 MHz, D$_2$O): δ (ppm) =7.46 (t, 1H, *J* = 7.6 Hz), 7.68 (d, 1H, *J* = 8.4 Hz), 8.30 (d, 1H, *J* = 6.8 Hz), 8.54 (s, 1H).

^{13}C-NMR (100 MHz, D$_2$O): δ (ppm) = 127.3, 130.7, 133.4, 138.5, 141.4, 167.3.

Elemental analysis: C, 52.17; H, 4.38; N, 20.28; O, 23.17.

Isonicotinamide-*N*-oxide: Yield % = 72; FT-IR (KBr, cm^{-1}): 464, 1395, 1495, 1685, 3157, 3349.

^{1}H-NMR (400 MHz, D$_2$O): δ (ppm) = 7.79 (d, 1H, *J* = 7.6 Hz), 8.26 (d, 1H, *J* = 6.8 Hz);

^{13}C-NMR (100 MHz, D$_2$O): δ (ppm) = 125.6, 134.2, 138.6, 178.1.

Elemental analysis: C, 52.17; H, 4.38; N, 20.28; O, 23.1.

Acridine-*N*-oxide: Yield % = 25; FT-IR (KBr, cm^{-1}): 750, 1304, 1417, 1575, 3073

^{1}H-NMR (400 MHz, CDCl$_3$): δ (ppm) = 7.53 (t, 1H, *J* = 7.6 Hz), 7.78 (t, 1H, *J* = 7.2 Hz), 8.00 (d, 1H, *J* = 8.4 Hz), 8.24 (d, 1H, *J* = 8.8 Hz), 8.78 (s, 1H).

^{13}C-NMR (100 MHz, D$_2$O): δ (ppm) = 118.0, 120.1, 126.1, 128.8, 131.5, 141.7

Elemental analysis: C, 79.98; H, 4.65; N, 7.17; O, 8.20.

4,4'-Bipyridine-*N,N*-dioxide: Yield % = 92; FT-IR (KBr, cm^{-1}): 834, 1240, 1320, 1468, 3063.

^{1}H NMR (400 MHz, D$_2$O): δ (ppm) = 7.85 (d, 1H, *J* = 7.6 Hz), 8.26 (d, 1H, *J* = 7.6 Hz);

^{13}C-NMR (100 MHz, D$_2$O): δ (ppm) = 123, 132, 139.

Elemental analysis: C, 63.82; H, 4.28; N, 14.89; O, 17.00.

2,2'-Bipyridine-*N,N*-dioxide Yield % = 70; FT-IR (KBr, cm^{-1}): 768, 1146, 1250, 1428, 1660, 3039.

^{1}H-NMR (400 MHz, DMSO-d_6): δ (ppm) = 7.61 (t, 2H), 7.70 (d, 1H, *J* = 8.4 Hz), 8.33 (d, 1H, *J* = 7.2 Hz)

^{13}C-NMR (100 MHz, DMSO-d_6): δ (ppm) = 128.4, 128.8, 131.5, 139.6, 141.7

Elemental analysis: C, 63.82; H, 4.28; N, 14.89; O, 17.00

Phenazine-*N,N*-dioxide: Yield % = 85; FT-IR (KBr, cm^{-1}): 766, 1092,1272, 1353

^{1}H-NMR (400 MHz, CDCl$_3$): δ (ppm) = 7.85 (t, 2H, *J* = 3.6 Hz), 8.77 (d, 2H, *J* = 3.2 Hz)

^{13}C-NMR (100 MHz, CDCl$_3$): δ (ppm) = 120.2, 131.3, 136.1

Elemental analysis: C, 67.92; H, 3.80; N, 13.20; O, 15.08.

1,10-Phenanthroline-*N,N*-dioxide: Yield % = 82; FT-IR (KBr, cm^{-1}): 898, 1263, 1486, 1574, 3076; 1H-NMR (400 MHz, CDCl$_3$): δ (ppm) = 7.40 (t, 1H, *J* = 8 Hz), 7.58 (d, 1H, *J* = 8 Hz), 7.99 (d, 1H, *J* = 7.6 Hz, 8.08 (s, 1H).

^{13}C-NMR (100 MHz, CDCl$_3$): δ (ppm) = 128.1, 129.3, 130.4, 132.6, 132.8, 134.0.

Elemental analysis: C, 67.92; H, 3.80; N, 13.20; O, 15.08.

2.B.6.4 DFT Calculation

Hydrogen bond synthon energies were calculated using Gaussian09, B3LYP/6-311G*(d,p) basis level of theory.

2.B.6.5 Vibrational Spectroscopy

For an initial characterization of synthesized pyridine *N*-oxides and drug cocrystals, melting point and FT-IR spectroscopy were employed. A Nicolet 6700 FT-IR spectrometer with an NXR FT-Raman Module was used to record the IR spectra on samples dispersed in KBr pellets. All major stretching frequencies for cocrystals (Figure 2.B.3), **C1** [PROP•BPNO]: 3270 (O–H), 3113 (C–H), 2958 (C– H), 1293 (C=N), 1237(N–O) cm^{-1}; **C2** [PABA•BPNO]: 3429 (O–H), 3355, 3241 (N–H), 1666 (C=O), 1328 (C=N), 1219 (N–O), 1028 (C–O) cm^{-1}; **C3** [FERU•BPNO]: 3470 (O–H), 3279 (N–H), 1687(C=O), 1305 (C=N), 1226 (N–O) cm^{-1}; **C4** [SULF•BPNO]: 3397, 3320 (N–H), 1595 (N–H$_{bending}$), 1270 (S=O), 1323 (C=N), 1227 (N–O), 838 (S–N, S–C) cm^{-1}.

2.B.7   NMR Spectroscopy

The chemical environments of *N*-oxides were determined by recording the ^{1}H and ^{13}C NMR spectra in JEOL JNM-ECS FTNMR equipped with a 5 mm SB dual ^{1}H/^{13}C probe and Delta software.

2.B.7.1 Differential Scanning Calorimetry (DSC))

The representative melting temperature onsets of the cocrystals and corresponding solvate/water release onsets if any are examined by thermal analysis (Figure 2.B.4). Details about the sample preparation technique and the instrument are described in Chapter 2 part A and the same procedure is followed.

2.B.7.2 Powder X-ray diffraction

Powder XRD of all samples was recorded on a Bruker D8 Focus X-Ray Diffractometer, Germany using Cu-Kα X-radiation (λ = 1.54056 Å) at 35 kV and 25 mA. Diffraction patterns were collected over a 2θ range of 10–50° at a scan rate of 5° min^{-1}. Rietveld refinement was performed using Powder Cell 2.3.

2.B.7.3   Single Crystal X-ray Diffraction

X-ray reflections were collected on a Bruker APEX-II, CCD diffractometer using Mo Kα (λ = 0.71073 Å) radiation [24]. Data reduction was performed using Bruker SAINT Software [25]. Intensities for absorption were corrected using SADABS. Structures were solved and refined using SHELXL-2014 with anisotropic displacement parameters for non-H atoms [26]. Hydrogen atoms on O and N are experimentally located in all crystal structures. All C–H atoms are fixed geometrically using the HFIX command in SHELX-TL. X-Seed is used to prepare figures and packing diagrams [27]. A check of the final CIF file using PLATON did not show any missed symmetry [28]. The hydrogen bond distances in the X-ray crystal structures are neutron-normalized by fixing the D–H distance to its accurate neutron value (O–H 0.983 Å, N–H 1.009 Å, C–H 1.083 Å). The hydrogen bond geometries are presented in Table 2.B.10.

2.B.7.4 Cambridge Structure Database (CSD)

A Cambridge Structural Database (ConQuest 1.18, build RC2, CSD version 5.37 February 2016 Updates, www.ccdc.cam.ac.uk) survey was performed to analyse

recurring supramolecular synthon formation by pyridine *N*-oxides with drug molecules containing different functionalities (Figure 2.B.10). The hydrogen-bonded synthon obtained from the organic cocrystal structures i.e. the CSD refcodes are listed in Table A.3.

2.B.7.5 Hirshfeld Surface Analysis

The Hirshfeld Surfaces offer characteristics of various types of intermolecular interactions by colour coding and contour diagrams. The 2D-fingerprint plot with unique colour generated from the Hirshfeld provides a 'fingerprint' of the different intermolecular interactions in the crystal and provides an understanding of various interactions (Figure 2.B.11 & 2.B.12). The analysis was carried out using the software Crystal Explorer 3.0.

2.B.8 References

[1] Albini, A. and Pietra, S. *Heterocyclic N-oxides*. CRC Press, 1991.

[2] Collado, D., Perez-Inestrosa, E., Suau, R., Desvergne, J.-P., and Bouas-Laurent, H. Bis(isoquinoline N-oxide) Pincers as a New Type of Metal Cation Dual Channel Fluorosensor. *Organic Letters*, 4(5):855–858, 2002.

[3] Malkov, A. V., Bell, M., Castelluzzo, F., and Kočovský, P. METHOX: A new pyridine N-oxide organocatalyst for the asymmetric allylation of aldehydes with allyltrichlorosilanes. *Organic Letters*, 7(15):3219-3222, 2005.

[4] Fulton, J. R., Glover, J. E., Kamara, L., and Rowlands, G. J. Facile synthesis of planar chiral N-oxides and their use in Lewis base catalysis. *Chem. Commun.*, 47(1):433-435, 2011.

[5] Schütznerová, E. and Krchňák, V. N-Oxide as an Intramolecular Oxidant in the Baeyer-Villiger Oxidation: Synthesis of 2-Alkyl-2H-indazol-3-yl Benzoates and 2-Alkyl-1,2-dihydro-3H-indazol-3-ones. *Journal of Organic Chemistry*, 81(9):3585-3596, 2016.

[6] Cerecetto, H., Dias, E., Di Maio, R., González, M., Pacce, S., Saenz, P., Seoane, G., Suescun, L., Mombrú, A., Fernández, G., and Lema, M. Synthesis and herbicidal activity of N-oxide derivatives. *Journal of Agricultural and Food Chemistry*, 48(7):2995-3002, 2000.

[7] Balzarini, J., Stevens, M., De Clercq, E., Schols, D., and Pannecouque, C. Pyridine N-oxide derivatives: Unusual anti-HIV compounds with multiple mechanisms of antiviral action. *Journal of Antimicrobial Chemotherapy*, 55(2):135-138, 2005.

[8] Stevens, M., Pannecouque, C., De Clercq, E., and Balzarini, J. Pyridine N-oxide derivatives inhibit viral transactivation by interfering with NF-κB binding. *Biochemical Pharmacology*, 71(8):1122-1135, 2006.

[9] Gonda, M., Nieves, M., Nunes, E., de Ceráin, A. L., Monge, A., Lavaggi, M. L., González, M., and Cerecetto, H. Phenazine N,N′-dioxide scaffold as selective hypoxic cytotoxin pharmacophore. Structural modifications looking for further DNA topoisomerase II-inhibition activity. *MedChemComm*, 4(3):595-607, 2013.

[10] Bull, J. A., Mousseau, J. J., Pelletier, G., and Charette, A. B. Synthesis of pyridine and dihydropyridine derivatives by regio- and stereoselective addition to n - activated pyridines. *Chemical Reviews*, 112(5):2642-2713, 2012.

[11] Babu, N. J., Reddy, L. S., and Nangia, A. Amide N-oxide heterosynthon and

amide dimer homosynthon in cocrystals of carboxamide drugs and pyridine N-oxides. *Molecular Pharmaceutics*, 4(3):417-434, 2007.

[12] Reddy, L. S., Babu, N. J., and Nangia, A. Carboxamide-pyridine N-oxide heterosynthon for crystal engineering and pharmaceutical cocrystals. *Chemical Communications*, (13):1369-1371, 2006.

[13] Goud, N. R., Babu, N. J., and Nangia, A. Sulfonamide−Pyridine-N-oxide Cocrystals. *Crystal Growth & Design*, 11(5):1930-1939, 2011.

[14] Rybarczyk-Pirek, A. J., Łukomska-Rogala, M., Wojtulewski, S., and Palusiak, M. N-Oxide as a Proton Accepting Group in Multicomponent Crystals: X-ray and Theoretical Studies on New p-Nitropyridine-N-oxide Co-Crystals. *Crystal Growth and Design*, 15(12):5802-5815, 2015.

[15] Saikia, B., Khatioda, R., Bora, P., and Sarma, B. Pyridine N-oxides as coformers in the development of drug cocrystals. *CrystEngComm*, 18(43):8454-8464, 2016.

[16] Du, M. and Zhao, X. J. 3-Carboxypyridine N-oxide: Supramolecular aggregation through O-H···O and C-H···O interactions. *Acta Crystallographica Section E: Structure Reports Online*, 59(11):o1645-o1647, 2003.

[17] Thaimattam, R., Reddy, D. S., Xue, F., Mak, T. C. W., Nangia, A., and Desiraju, G. R. Interplay of strong and weak hydrogen bonding in molecular complexes of some 4,4′-disubstituted biphenyls with urea, thiourea and water. *Journal of the Chemical Society, Perkin Transactions 2*, 0(8):1783-1790, 1998.

[18] Rozen, S. and Dayan, S. At Last, 1,10-Phenanthroline-N,N'-dioxide, A New Type of Helicene, has been Synthesized using HOF small middle dotCH(3)CN. *Angewandte Chemie International Edition*, 38(23):3471-3473, 1999.

[19] Baker, M. T. and Naguib, M. Propofol: the challenges of formulation. *Anesthesiology*, 103(4):860-876, 2005.

[20] McKellar, S. C., Kennedy, A. R., McCloy, N. C., McBride, E., and Florence, A. J. Formulation of liquid propofol as a cocrystalline solid. *Crystal Growth and Design*, 14(5):2422-2430, 2014.

[21] Moreno-Fuquen, R., Font i Carot, M., Garriga, M., Cano, F., Martinez-Ripoll, M., Valderrama-Naranjo, J., and Serratto, L. M. The 2:1 complex of 4-aminobenzoic acid and 4,4′-bipyridyl N,N'-dioxide. *Acta Crystallographica Section E Structure Reports Online*, 59(4):o495-o497, 2003.

[22] Munroe, Á., Rasmuson, Å. C., Hodnett, B. K., and Croker, D. M. Relative stabilities of the five polymorphs of sulfathiazole. *Crystal Growth and Design*,

12(6):2825-2835, 2012.

[23] Spackman, M. A. and Jayatilaka, D. Hirshfeld surface analysis. *CrystEngComm*, 11(1):19-32, 2009.

[24] *BRUKER AXS (v 6.14); Bruker AXS Inc.: Madison, WI.* 2008.

[25] *SAINT Plus, Bruker AXS Inc.: Madison, WI.* 2008.

[26] Sheldrick, G. M. *SHELXS97 and SHELXL97: Programs for Crystal Structure Solution and Refinement University of Göttingen.* 1997.

[27] L. J. Barbour *X–Seed, Graphical Interface to SHELX–97 and POVRay University of Missouri–Columbia.* 1999.

[28] Spek, A. L. *PLATON, A Multipurpose Crystallographic Tool Utrecht University, Utrecht, Netherland.* 2002.